Egypt. J. Chem. Vol. **68**, No.2, pp. 537 -560 (2025)

Egyptian Journal of Chemistry

http://ejchem.journals.ekb.eg/

Synthesis, Characterization, and Multifaceted Applications of Co(II) and Cu(II) Hydrazono Schiff Base Complexes: Integrating DFT, Molecular Docking, Biomedical Studies, and Nanotechnology-Enhanced Cadmium Detection Using Hydrazono Copper Complex-Based QCM

Ali A. Mohamed [1*], Rabab M. El-Sherif [2], Walaa H. Mahmoud [1], Ahmed A. El-Sherif [1]

[1] *Chemistry Department, Faculty of Science, Cairo University, Giza, 12613 Egypt*
[2] *Faculty of Postgraduate Studies for Nanotechnology, Cairo University, Zayed City, Giza, Egypt*

Abstract

This study explores the synthesis and multifaceted applications of a novel Schiff base ligand, (HYD) (1E,2E)-N-(4-methoxyphenyl)-1-(2-(p-tolyl)hydrazono)propan-2-imine, and its binary complexes with cobalt (II) and copper (II) ions. The compounds were extensively characterized using various spectroscopic and analytical techniques. Density Functional Theory (DFT) calculations suggested a distorted octahedral geometry for these complexes. The antimicrobial properties of the synthesized compounds were evaluated against a range of bacterial and fungal strains, with the copper (II) complex exhibiting superior efficacy. The antitumor potential was assessed against MCF-7 breast carcinoma cells. Molecular docking simulations provided insights into the binding interactions with protein receptors (7DAF), informing future inhibition studies. This research introduces a nanotechnology-based approach for detecting cadmium pollution in environmental samples. The nanostructured copper (II) Schiff base complex was analyzed using advanced techniques, including XRD, SEM, AFM, and BET surface area analysis. A quartz crystal microbalance (QCM) sensor incorporating this nano complex demonstrated high sensitivity in detecting Cd(II) ions in groundwater and industrial effluent wastewater samples, with rapid results obtained in under 5 minutes. The sensitivity of the QCM-based sensor was investigated under various pH levels and temperatures, showcasing its versatility in different environmental conditions. Additionally, the cytotoxic effects of nanoparticles derived from the copper (II) Schiff base complex were studied to assess their biocompatibility. This comprehensive study highlights the versatile applications of the synthesized compounds as potential antimicrobial and anticancer agents, as well as their promising role in developing sensitive, efficient nanosensors for rapid and accurate environmental cadmium detection. The research underscores the potential of integrating nanotechnology with traditional chemical approaches to address pressing environmental and health challenges.

Keywords: Nanosensor; Nano complex; SEM; BET; AFM; DFT; Docking; QCM

I. Introduction

Schiff bases and their metal complexes have emerged as a prominent class of compounds in modern coordination chemistry owing to their exceptional versatility and wide-ranging applications [1,2]. These organic ligands are synthesized through a condensation reaction between primary amines and carbonyl compounds, forming a characteristic azomethine (-C=N-) functional group [3]. This unique structural moiety enables Schiff bases to act as multidentate chelating agents, capable of forming stable complexes with various transition metals, exhibiting diverse electronic, magnetic, and biological properties [4,5]. Among the transition metal ions, those belonging to the first row of the periodic table, particularly cobalt(II) and copper(II), have garnered significant interest due to their ability to form complexes with Schiff base ligands [6,7]. These metal ions can adopt different oxidation states and coordination geometries, enhancing the resulting complexes' reactivity, stability, and potential applications. This flexibility in coordination chemistry has opened up a broad spectrum of applications, ranging from catalysis and material science to medicinal chemistry and biotechnology [8,9]. Cobalt(II) complexes with Schiff bases have demonstrated promising biological activities, including antimicrobial, antifungal, and anticancer properties [10]. Cobalt is an essential trace element in biological systems, playing a crucial role in vitamin B12 metabolism and various enzymatic processes [11]. The formation of these complexes involves the coordination of the cobalt(II) ion with the azomethine nitrogen and other donor atoms (e.g., oxygen, sulfur) present in the Schiff base framework [14,15]. The unique electronic configuration of cobalt, combined with the structural flexibility of Schiff bases, results in complexes exhibiting diverse coordination geometries, such as tetrahedral, square planar, and octahedral arrangements. These geometries significantly influence the complexes' reactivity, stability, and biological activity [12,13]. Similarly, copper is another biologically and therapeutically significant transition metal that forms complexes with Schiff bases [16,17]. Copper plays a vital role in various biological functions, including enzymatic reactions, redox processes, and the maintenance of healthy connective tissues [18,19]. Copper(II) complexes with Schiff bases have been extensively studied due to their remarkable biological activities and potential medical applications. These complexes

*Corresponding author e-mail: alimoftah9191@gmail.com, (Ali A. Mohamed).
Receive Date: 17 June 2024, Revise Date: 01 August 2024, Accept Date: 03 August 2024
DOI 10.21608/ejchem.2024.297906.9872

have demonstrated promising antimicrobial, antifungal, and anticancer properties, making them attractive candidates for therapeutic applications [20,21]. Additionally, Schiff base complexes of copper have found applications in catalysis, sensor development, and materials science [8,9]. Schiff base metal complexes' unique properties and potential applications have driven extensive research efforts to synthesize and characterize novel compounds. Researchers aim to unravel their structure-activity relationships and explore their suitability for diverse applications. Through careful design and modification of the ligand frameworks, researchers strive to fine-tune these complexes' electronic and steric properties, enhancing their performance and expanding their scope of applications [4,5]. These complexes exhibit potent antimicrobial activity against many bacterial and fungal pathogens. The antimicrobial mechanism often involves interaction with microbial cell membranes, disruption of cellular processes, and inhibition of essential enzymes. Additionally, these complexes have shown promising anticancer activity by inducing cytotoxic effects in cancer cells through various mechanisms, including generating reactive oxygen species (ROS), interacting with DNA, and inhibiting topoisomerases, leading to cell cycle arrest and apoptosis [22]. Various analytical and characterization techniques are employed to comprehensively understand Schiff base metal complexes' properties and potential applications. These techniques provide crucial information about the complexes' composition, structure, and stability. Common techniques include elemental analysis, UV-visible spectroscopy, FT-IR spectroscopy, mass spectrometry, and conductometric measurements. Advanced computational methods, such as Density Functional Theory (DFT) calculations, are also employed to investigate the electronic properties, HOMO-LUMO energy gaps, dipole moments, and chemical hardness of Schiff base metal complexes [23]. For example, in this study, DFT calculations using the LANL2DZ basis sets and the B3LYP exchange-correlation functional were performed to predict the distorted octahedral geometry of the synthesized complexes [24]. Molecular docking studies complement the characterization process by elucidating Schiff base metal complexes' potential binding orientations and interaction patterns with various biological targets. Using the Molecular Operating Environment (MOE) program [25], docking simulations are conducted to assess the binding affinities and preferred modes of interaction of the Hydrazono Schiff base (HYD) and its Cu (II) complex with specific protein receptors. These studies are critical for understanding the molecular basis of the observed biological activities and guiding the design of more effective therapeutic agents. Nanotechnology is revolutionizing various fields, including environmental monitoring, by offering innovative solutions for detecting and mitigating pollutants [26, 27]. Nanotechnology enables the design and fabrication of nanosensors with unparalleled accuracy and sensitivity for detecting contaminants, particularly heavy metals like cadmium (Cd). Cadmium is a toxic heavy metal that poses significant environmental and health risks due to its persistence and bioaccumulation [28- 30]. Traditional methods for detecting Cd pollution often lack the sensitivity and real-time capabilities needed for effective environmental surveillance [31]. In this context, nanotechnology offers a transformative approach to environmental monitoring by providing highly sensitive and selective detection methods. Nanosensors are analytical devices that utilize nanomaterials to detect and quantify specific analytes with high sensitivity and selectivity. The high surface-to-volume ratio of nanomaterials enhances the sensitivity and specificity of nanosensors, enabling the detection of trace amounts of contaminants in various environmental matrices [32]. In cadmium detection, nanosensors based on nanostructured materials, such as copper (II) Schiff base complexes, have shown remarkable potential. These nanosensors can rapidly and accurately identify even trace amounts of cadmium in soil, water, and industrial effluent samples. Integrating nanotechnology into sensor design significantly enhances the performance and reliability of environmental monitoring systems [33]. The quartz crystal microbalance (QCM) technique is a highly sensitive method used to measure mass changes on a sensor surface by monitoring the frequency shifts of a quartz crystal resonator. QCM is particularly advantageous for detecting heavy metals like cadmium because it allows for real-time monitoring, high sensitivity, and cost-effectiveness [34]. When combined with nanostructured materials, such as copper (II) Schiff base complexes, QCM can achieve remarkable detection capabilities. The nanostructured copper(II) Schiff base complex exhibited a high affinity for cadmium ions, making it a promising material for developing a sensitive and rapid detection method for cadmium in environmental samples. The quartz crystal microbalance (QCM) technique evaluated the complex's sensitivity towards cadmium ions [35]. This technique monitors the frequency shifts of a quartz crystal resonator as mass changes occur on its surface due to the binding of target analytes. The comprehensive characterization of the nanostructured copper(II) Schiff base complex involved using advanced analytical techniques to unravel its intricate structural and physicochemical properties. X-ray Diffraction (XRD), Scanning Electron Microscopy (SEM), Atomic Force Microscopy (AFM), Fourier-Transform Infrared (FTIR) Spectroscopy, Dynamic Light Scattering (DLS), Zeta Potential Analysis, BET Surface Area, and Pore Size Determination were employed to gain insights into the complex's structure, morphology, surface properties, and porosity. The combination of the nanostructured copper(II) Schiff base complex's high affinity for cadmium ions and the high sensitivity of the QCM technique enabled the rapid and precise detection of cadmium in various environmental samples. This approach demonstrated the ability to detect and quantify Cd(II) ions in groundwater and industrial effluent wastewater samples with high sensitivity and rapid response times, highlighting its potential for environmental monitoring and remediation applications. This study highlights Schiff base metal complexes' versatile applications and promising bioactive properties. The synthesized compounds exhibit significant antimicrobial and anticancer activities and are effective nanosensors for environmental monitoring, showcasing their potential for further development and application in various scientific and industrial fields. Integrating nanotechnology into the design and application of Schiff base metal complexes represents a significant advancement in coordination chemistry and environmental science. As the field continues to evolve, developing more sophisticated nanosensors and therapeutic agents based on Schiff base metal complexes will undoubtedly contribute to addressing some of the most pressing challenges in healthcare and environmental protection.

II. Experimental Section

2.1. Chemicals and Experimental Procedures

This research used high-purity chemicals to guarantee accurate synthesis and characterization of the target compounds. The primary starting materials included 4-methoxy aniline with a purity of 98% and (E)-1-(2-(p-

tolyl)hydrazineylidene) propan-2-one with a purity of 99%, both sourced from Sigma Aldrich, a well-known supplier of chemical reagents. To synthesize the metal complexes, we used Cobalt(II) chloride hexahydrate ($CoCl_2.6H_2O$, 98% purity) and Copper chloride hydrate ($CuCl_2.2H_2O$, 99.99% purity), obtained from BDH, a trusted supplier of high-quality chemicals. Absolute ethanol (Ethyl alcohol, 99.9% purity), a spectroscopic-grade organic solvent, was also procured from BDH to facilitate the synthesis and purification. Throughout the experimental procedures, bidistilled water produced using glass distillation equipment was consistently used to ensure the highest purity and reduce the risk of contamination. The choice of materials and methods in this study was made with great care to ensure the quality and reproducibility of the research results, adhering to established protocols and best practices in both synthetic chemistry and biological evaluation.

2.1.1. Solutions

Reservoir solutions containing the (**HYD**), and their corresponding metal complex, each formulated at a specific concentration of 1 X 10^{-3} M, were created by precisely dissolving the appropriate weight in ethanol for Schiff base ligand (**HYD**), Co(II) and Cu (II) complex. The conductivity of the 1 X 10^{-3} M metal complex solution was then measured. Subsequently, solutions of the (**HYD**) and its Binary (Co (II) and Cu (II)) complexes were diluted to a concentration of 1 X 10^{-4} M, utilizing precise dilution techniques from the initially prepared reservoir solutions for UV–Vis spectra measurement.

2.2. Instrumentation

This investigation, conducted at Cairo University in Egypt, employed a multifaceted analytical approach to characterize various materials comprehensively. Various scientific instruments and techniques were utilized to explore the investigated substances' intrinsic properties and distinctive features. Elemental analysis was performed using a LECO CHNS-932 Vario Elemental Analyzer at Cairo University's Microanalytical Center. This helped determine the samples' carbon, hydrogen, and nitrogen content. Melting points were measured with a triforce XMTD-3000 apparatus [36]. Fourier transform infrared (FTIR) spectroscopy was conducted from 4000 to 400 cm^{-1} using a PerkinElmer 1650 spectrometer with KBr disks. The molar conductance of solid complex solutions in 10^{-3} M ethanol was assessed using a Jenway 4010 conductivity meter [37]. Mass spectrometry applied electron ionization at 70 eV with a Hewlett-Packard MS-5988 GS-MS—spectral analysis from 200 to 700 nm utilized a PerkinElmer Model spectrophotometer for solutions. Additional characterization included antimicrobial studies at Cairo University's Microanalytical Center and cytotoxicity research at the adjacent National Cancer Institute. Malvern Panalytical NanoSight NS500 determined nano Copper complexes' particle size and surface charge. After degassing metal complex nanoparticles, BET surface area/pore volume analysis employed a Quanta Chrome Nova Touch 4L. Morphology was characterized using Oxford's Jupiter XR AFM model [38]. Samples underwent 10-minute ultrasonication before TEM analysis. Thin film synthesis applied a Laurell-650Sz Spain coater under vacuum. AFM images/roughness profiles at 47 nm employed contact mode scanning. Mass spectra were acquired using a Hewlett-Packard MS-5988 GS-MS instrument, which employed electron ionization at 70 electron volts (eV). Spectra in the 200-700 nm wavelength range for solutions were recorded on a PerkinElmer Model UV-Vis spectrophotometer [39]. Antimicrobial studies were conducted at Cairo University's Microanalytical Center, while cytotoxicity research was performed at the adjacent National Cancer Institute, also located at Cairo University. Surface charge and particle size characterization of the nano Copper complex was carried out using a Malvern Panalytical NanoSight NS500 instrument. BET surface area and pore volume analysis employed a Quanta Chrome Nova Touch 4L surface area and pore volume analyzer via multi-point and DH pore volume methods after degassing the metal complex nanoparticles at 65°C for 1.25 hours [40]. The morphology of the Copper complex nanoparticles was analyzed via AFM using an Oxford Jupiter XR AFM model. Samples underwent 10 minutes of sonication before TEM analysis using a UP400S ultrasonic probe sonicator (Hielscher, Oderstraße, Teltow, Germany) at 55 kHz amplitude, 55% cycle and 0.55 amplitude [41]. Thin film synthesis applied a Laurell-650Sz vacuum coater from Spain at 750 rpm rotational speed and 50μm rate over 120 seconds. AFM images and roughness profiles were obtained at 47 nm x 47 nm dimensions using contact mode with a gold tap and 0.31 In/s scanning speed. This allowed a detailed examination of surface characteristics and morphology of the nickel complex nanoparticles, providing insights into structural features. Thin films were fabricated using a Laurell650Sz vacuum coater apparatus (France), maintaining 750 rpm rotational speed and depositing 50 μm every 120 seconds [42]. Surface wettability was evaluated using a Biolin Scientific T200 contact angle analyzer in a sessile drop configuration. Assessments used 10-second intervals with 4 μL droplets of distilled water. In developing Copper complex nanosensors based on quartz crystal microbalance (QCM), an AT-cut 5 MHz quartz crystal chip with a 12 mm gold electrode (Q-Sense, Shenzhen, China) was used. The gold sensor underwent cleaning by immersing in aqueous ammonia, H2O2, and double-distilled water (5:1:1 v/v/v) at 75°C for 10 minutes, then rinsing with double-distilled water and ethanol before air-drying at room temperature [37-43]. The dried chip was inserted into the Q-Sense instrument. Double-distilled water was introduced as a background electrolyte to obtain baseline measurements before incorporating nanomaterials. A continuous infusion of double-distilled water stabilized the QCM signal at zero. Then, 2 mL of 2 ppm cadmium complex nanoparticles were prepared by mixing with 10 mL double-distilled water, and a portion was carefully introduced onto the gold sensor at 0.4 mL/min flow rate [43].

2.2.1. Preparation and Structural Elucidation of a Novel Hydrazono Ligand (HYD)

Building upon previous work synthesizing new Schiff base complexes, a new Schiff base ligand (**HYD**) was prepared via a standard condensation method [44, 45]. The synthesis involved reacting 4-methoxyaniline (2.435 mmol, 0.3 g) with (E)-1-(2-(p-tolyl)hydrazineylidene)propan-2-one (2.435 mmol, 0.429 g) in hot ethanol (100%) at 60-65°C in a round-bottom flask. The mixture was refluxed for 4 hours in an open system under controlled laboratory conditions to ensure thorough mixing, allowing the condensation reaction to take place and form the Schiff base ligand. After cooling to room temperature, a golden-yellow solid was obtained. The resulting Schiff base ligand was isolated with a yield of 88% after filtration and recrystallization. Scheme (1) illustrates the structure of the Schiff base ligand (HYD) and the formation reaction involved in its synthesis. The final product was an orange solid with a melting point of 223°C and a yield of 79%. The theoretical composition for the molecular formula $\mathbf{C_{17}H_{19}N_3O}$ was calculated to be Carbon (C) 72.57%, Hydrogen (H) 6.81%, and Nitrogen (N) 14.94%.

Experimental elemental analysis results closely matched these values, showing Carbon (C) at 72.13%, Hydrogen (H) at 6.33%, and Nitrogen (N) at 14.19%. Fourier-transform infrared (FT-IR) spectroscopy analysis revealed characteristic absorption bands at ν = 3419 cm-1 (attributed to N-H stretching) and 1635 cm-1 (assigned to C=N stretching). Ultraviolet-visible (UV-Vis) spectroscopy showed distinct absorption bands at wavelengths of 271 nm (attributed to π–π* transitions), 306 nm (indicative of n–π* transitions), and 378 nm (associated with charge transfer transitions). The characterization data, including melting point, elemental analysis, FT-IR, and UV-Vis spectroscopy, confirmed the successful synthesis of the (**HYD**), providing valuable insights into its molecular structure and electronic properties.

2.2.2 Synthesis of Hydrazono Binary Complexes and its Nano Structure of Cu (II) complex

The binary metal complexes were synthesized using the previously prepared (**HYD**). The (**HYD**) ligand (0.842 mmol, 0.2369 g) has been dissolved in 50 mL of hot absolute. The metal chelates were formed by combining the hot ethanolic solution of the (**HYD**) with a hot ethanolic solution (15 mL) of the respective metal chloride salt ($CoCl_2.6H_2O$ and $CuCl_2.2H_2O$) (0.842 mmol). The metal salt solution was then added dropwise to the (**HYD**) solution under fixed stirring to facilitate the complexation reaction. The resulting reaction mixture underwent reflux for Four hours at (60-65°C), during which time the formation of precipitates occurred, indicating the complexation of the metal ions with the (**HYD**). The precipitated complexes were filtrated and purified through multiple washings with ethanol and water to remove unreacted starting materials or by-products. Finally, the purified complexes were dried in a vacuum desiccator over anhydrous calcium chloride ($CaCl_2$) to remove residual solvents. Scheme (1) illustrates the binary metal complexes' general structure and formation reaction. The synthesis of these complexes involved the coordination of the (**HYD**) with the respective metal ions (Co(II) and Cu(II)) through the formation of metal-ligand bonds, resulting in the desired binary metal complexes. The synthesized Cu(II) complex was also subjected to 10 minutes of ultrasonic probe treatment to convert the Schiff base copper complex to nanoscale. This resulted in a discernible color change from dark green to green hue [45].

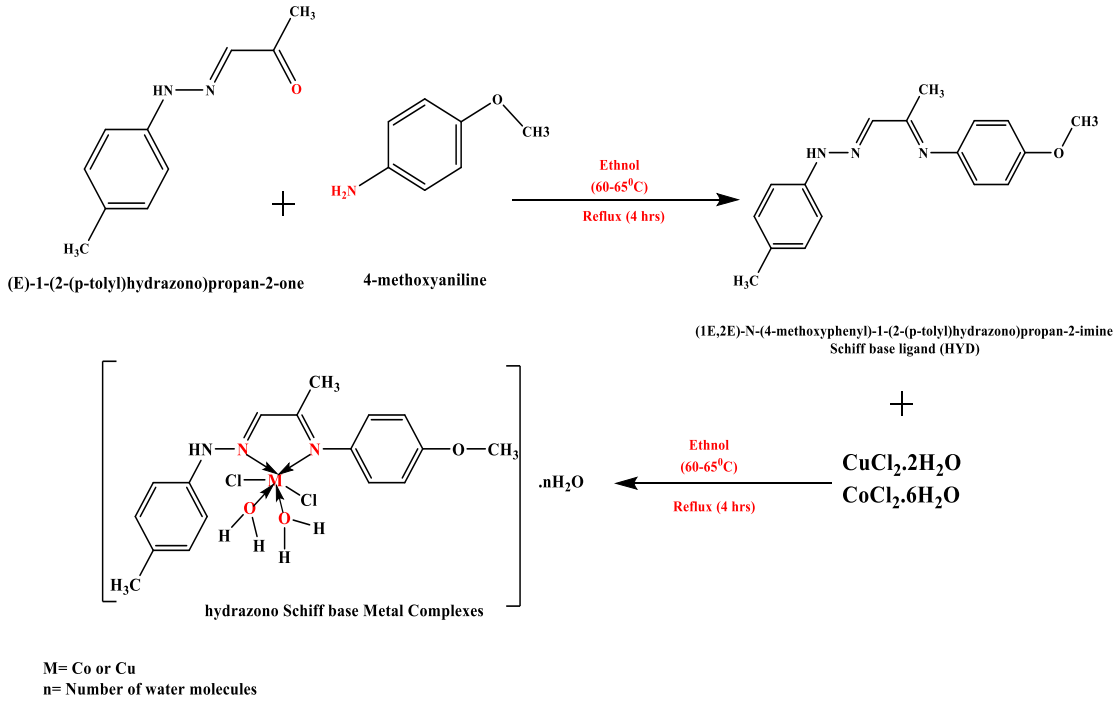

Scheme 1. Synthesis pathway of Schiff base ligand **(HYD)** and its metal complexes.

2.3. Computational methodology

The electronic structure calculations of the (**HYD**) and its Cu (II) complex were performed using the Gaussian09 software package. Both structures were fully optimized using density functional theory (DFT) with the hybrid B3LYP functional. We employed a mixed approach for the basis set to ensure an accurate representation of all atoms in the system. The LANL2DZ basis set was used for the Cu atom in the complex, as it is particularly suitable for transition metals. In contrast, for the ligand atoms (C, H, N, O) in both the (**HYD**) and its Cu(II) complex, we utilized the 6-31G(d,p) basis set, which is appropriate for main group elements. This combination of basis sets was chosen to obtain the Geometry Optimized Structures of the Hydrazono Schiff base ligand (**HYD**) and its Cu (II) complex and to calculate different functional parameters like Total Energy, Dipole Moment, E_{HOMO}, E_{LUMO}, Band Gap Energy ($\Delta E = E_{HOMO} - E_{LUMO}$), Electron Affinity, Electro-negativity and Electrostatic maps (MEP) [46]. The optimized molecular electrostatic potential (MEP) reveals the reactive sites within the

molecule. Electrophilic reactivity, characterized by negative potential, is depicted in red, while nucleophilic reactivity, indicated by positive potential, is represented in blue.

2.4. Molecular docking study

Molecular docking analysis has been managed using the MOE 2014 software package to investigate the interaction between the (Hydrazono Schiff base ligand (**HYD**) and its Cu (II) complex) and a target macromolecule relevant to cancer treatment [47]. The protein's three-dimensional structure has been obtained from the Protein Data Bank (PDB) website (**PDB: 7DAF**). The optimal structure of the complex was generated using Gaussian 09 software with the B3LYP method, followed by docking them to the target receptor. The interaction between the protein and ligands was also analyzed using MOE software.

2.5. Monitoring Cadmium Ion Levels through QCM

The Quartz Crystal Microbalance (QCM) evaluations were performed using a QCM instrument from Q-Senses, Biolin Scientific, located in Linthicum Heights, MD, USA. Each measurement involved introducing 1 ppm cadmium solutions onto QCM-based copper nanosensors designed for cadmium complex detection (Fig 1) [48]. Measurements were systematically conducted under varying conditions: Temperature (25°C, 35°C, 45°C) and pH (3.5, 7, 11). The cadmium solution was administered until the signal stabilized, indicating equilibrium binding between the nanosensors and cadmium ions [49]. Double-distilled water was introduced into the system after a time interval to purge non-adsorbed particles from the QCM sensor interfaces. This was done to eliminate any remaining cadmium particles and optimize the nanosensors for subsequent measurements [50].

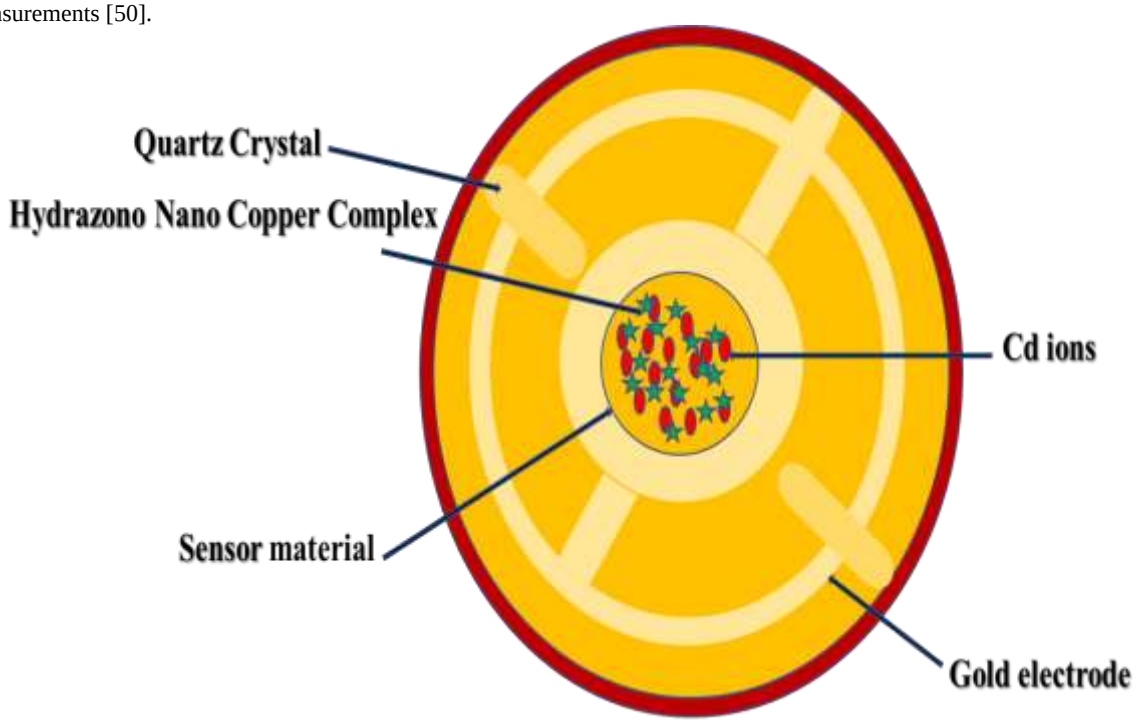

Fig 1. QCM Monitoring Setup for Cadmium Ion Binding to Nano-Sized Hydrazono Copper Complex Sensors

III. Results and Discussion

3.1. Characterization of Hydrazono Schiff base (HYD) and its Binary Complexes

3.1.1. Elemental analyses and Molar conductance

Two metal complexes were synthesized via the combination of equimolar quantities of the (**HYD**) with cobalt(II) and copper(II) metal salts in suitable solvents. Detailed elemental analyses and an exploration of these compounds' molecular formulae, melting points, and various physical properties were conducted. These complexes demonstrated stability at room temperature and exhibited high sharp melting points. They were determined to exhibit limited solubility in water and high solubility in DMSO solvents. The estimated values and the experimental elemental analysis of the complexes demonstrated a remarkable level of agreement. As indicated in Table 1, the complexes prominently manifest a 1:1 ratio, wherein a single metal ion forms Two bonds with one Schiff base (**HYD**) ligand. Consequently, this outcome gives rise to a complex with stoichiometry denoted as **(M)**: **(HYD).**

Table 1. Analytical and Physical Data for the Cobalt(II) and Copper(II) Complexes with (**HYD**)

Compound	Color Yield (%)	M.p. (°C)	Found (Calc.) C (%)	H (%)	N (%)	Cl (%)	M(%)	A_m (Ω^{-1} mol^{-1} cm^2)
(HYD) ($C_{17}H_{19}N_3O$)	Golden yellow (79)	223	72.13 (72.57)	6.33 (6.81)	14.19 (14.94)	…….	…….	…….
[Co(HYD)Cl_2(H_2O)$_2$].3H_2O $C_{17}H_{29}Cl_2CoN_3O_6$	Golden Green (84)	277	40.47 (40.73)	5.51 (5.83)	8.02 (8.38)	13.92 (14.14)	11.62 (11.76)	36
[Cu(HYD)Cl_2(H_2O)$_2$].H_2O $C_{17}H_{25}Cl_2CuN_3O_4$	Dark Green (82)	250	43.25 (43.46)	5.15 (5.36)	8.72 (8.94)	14.84 (15.09)	13.26 (13.52)	24

3.1.2. Mass Spectroscopy

The mass spectrometry analysis provides the calculated and found m/z values for the molecular ion peaks, offering insights into these compounds' successful formation and stability. For the hydrazono Schiff base (**HYD**) with the molecular formula **$C_{17}H_{19}N_3O$**, the calculated m/z value is 281.36, closely matching the found m/z value of 281.15. This slight difference between the calculated and found values is within the acceptable range for mass spectrometry measurements, indicating the successful synthesis and stability of the ligand. The presence of a molecular ion peak at m/z 281.15 confirms the integrity of the ligand molecule. In the case of the cobalt complex **[Co(HYD)Cl_2(H_2O)$_2$].3H_2O** with the molecular formula **$C_{17}H_{29}Cl_2CoN_3O_6$**, the calculated m/z value is 501.27, while the found m/z value is 502.10. The observed peak is interpreted as $[M+1]^+$, indicating the addition of a proton (H+), a common occurrence in mass spectrometry due to the ionization process. The close match between the calculated and found m/z values supports the successful formation of the cobalt complex. The slight discrepancy of less than one unit can be attributed to the ionization process and is typical in such analyses. For the copper complex **[Cu(HYD)Cl_2(H_2O)$_2$].H_2O** with the molecular formula **$C_{17}H_{25}Cl_2CuN_3O_4$**, the calculated m/z value is 469.85, and the found m/z value is 468.80. The molecular ion peak at m/z 468.80 closely corresponds to the calculated value, indicating the presence of the copper complex. The minor deviation between the calculated and found values is within the acceptable range. It does not affect the interpretation of the data, confirming the formation and stability of the copper complex. Overall, the mass spectrometry data presented in this table provide essential information on the molecular weights of the synthesized compounds. As summarized in Table 2, the close agreement between the calculated and found m/z values for all three compounds demonstrates the synthesis processes' accuracy and the resulting products' stability. The slight deviations observed are typical in mass spectrometry and do not significantly impact the overall interpretation. These results confirm the successful formation of the (**HYD**) and its cobalt and copper complexes, validating the synthetic strategies used in their preparation.

Table 2. EI- mass data of Hydrazono Schiff base (**HYD**) and its metal complexes.

Compound	m/z value Calculated	Found	Interpretation
Hydrazono Schiff base (HYD) ($C_{17}H_{19}N_3O$)	281.36	281.15	$[M]^+$
[Co(HYD)Cl_2 (H_2O)$_2$]. 3H_2O $C_{17}H_{29}Cl_2CoN_3O_6$	501.27	502.10	$[M+1]^+$
[Cu (HYD)Cl_2 (H_2O)$_2$]. H_2O $C_{17}H_{25}Cl_2CuN_3O_4$	469.85	468.80	$[M]^+$

3.1.3. Spectrophotometric studies

The UV-visible absorption spectra of the (**HYD**) and its metal complexes were recorded in the wavelength range of 200-700 nm at room temperature using DMSO as the solvent. Solutions with a 10-4 M concentration were prepared for the spectral measurements. The free (HYD) ligand exhibited three distinct absorption bands in the UV-visible region, located at approximately 271 nm, 306 nm, and 378 nm. The band at 271 nm was assigned to a π→π* electronic transition, while the 306 nm band was attributed to a conjugated π→π* transition. The absorption at 378 nm was ascribed to an n→π* intraligand electronic transition. Upon complexation with cobalt and copper ions, shifts in the n→π* and π→π* transition bands were observed. In the cobalt complex, these bands appeared at 239 nm, 315 nm, and 365 nm, related to the π→π* conjugated, π→π*, and n→π* transitions, respectively. The bands were detected at 261 nm, 285 nm, 339 nm, and 395 nm for the copper complex. These spectral shifts indicate that the (**HYD**) coordinated with the metal ions by forming coordination bonds. A charge transfer band was also observed in the copper complex at 395 nm [44, 51], as summarized in Table 3.

Table 3. UV-Visible Absorption Spectral Data for the (HYD) and Its (Cobalt and Copper) Complexes.

Compound	Wavelength (nm)	Type of transition
Hydrazono Schiff base (HYD) ($C_{17}H_{19}N_3O$)	271,306, 378	$(\pi\rightarrow \pi^*)_{Conjugated}, \pi\rightarrow \pi^*, n\rightarrow\pi^*$
[Co(HYD)$Cl_2(H_2O)_2$].3H_2O $C_{17}H_{29}Cl_2CoN_3O_6$	239,315,365	$(\pi\rightarrow \pi^*)_{Conjugated}, \pi\rightarrow \pi^*, n\rightarrow\pi^*$
[Cu(HYD)$Cl_2(H_2O)_2$].H_2O $C_{17}H_{25}Cl_2CuN_3O_4$	261,285, 339, 395	$(\pi\rightarrow \pi^*)_{Conjugated}, \pi\rightarrow \pi^*, n\rightarrow\pi^*$, charge transfer

3.1.4. IR Spectral Studies

Infrared spectroscopy investigated the coordination behavior of the cobalt and copper complexes with the Hydrazono Schiff base ligand (**HYD**). The IR spectra showed that the metal ions coordinated with the azomethine groups' nitrogen atoms in the ligand [52]. A strong band corresponding to the (C=N) azomethine stretching vibration was observed in the free (**HYD**) ligand at 1634 cm^{-1}. Upon complexation, this band underwent a shift, appearing at 1617 cm^{-1} in the cobalt complex and 1612 cm^{-1} in the copper complex [53]. This shift towards lower wavenumbers indicates the coordination of the metal ions through the nitrogen donors. Additionally, new bands emerged in the spectra of the metal complexes, which were absent in the spectrum of the free ligand. A band at 483 cm^{-1} was assigned to the υ(M-N) vibration for the cobalt complex, confirming the formation of cobalt-nitrogen bonds. Furthermore, a band at 558 cm^{-1} was attributed to υ(M-O) vibrations from the coordinated water molecules. In the case of the copper complex, the υ(M-N) vibration appeared at 488 cm^{-1}, while the υ(M-O) vibration was observed at 588 cm^{-1} [53]. These results, summarized in Table 4 and illustrated in Figure 2, confirm that both cobalt and copper ions are coordinated to the Hydrazono Schiff base ligand through the azomethine nitrogen atoms [54].

Table 4. Prominent Infrared Spectral Data for the (**HYD**) and Its (Cobalt and Copper) Complexes**.**

Compound	υ(NH)	υ(C=N)	υ(M−N)	υ(M-O)
Hydrazono Schiff base (HYD) ($C_{17}H_{19}N_3O$)	3419	1634sh.	–	–
[Co(HYD)$Cl_2(H_2O)_2$].3H_2O $C_{17}H_{29}C_{l2}CoN_3O_6$	3420	1617sh	483	558
[Cu (HYD)Cl_2 (H_2O)$_2$].H_2O $C_{17}H_{25}Cl_2CuN_3O_4$	3425	1612 s	488 s	588 s

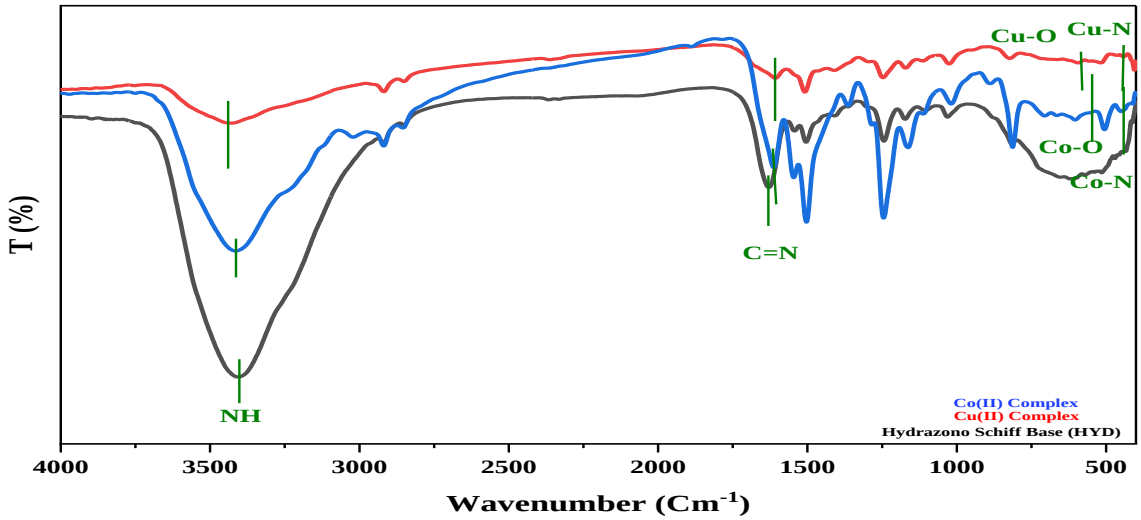

Fig 2. Infrared Spectra of the (HYD) and Its (Cobalt and Copper) Complexes.

3.1.5. Thermal analyses

The study utilized Thermal Gravimetric Analysis (TGA) to assess the synthesized metal complexes' thermal resilience and distinguish between water molecules existing as hydrated or coordinated within their structures [55-58]. Analysis through TG and DTG was conducted on the Hydrazono Schiff base ligand metal complexes, examining their behavior across a temperature spectrum from ambient conditions to 800°C. The thermal analysis of the **$[Co(HYD)Cl_2(H_2O)_2].3H_2O$** complex exhibited four decomposition steps. The initial step, between 35-110°C with a peak at 97.8°C, led to the loss of hydrated water molecules, estimating a mass loss of 10.16% (calculated = 10.782%). The subsequent step, between 110-465°C with a peak at 366.11°C, involved the loss of **$C_7H_{12}Cl_2NO$** with an estimated mass loss of 38.59% (calculated = 39.314%). The third step, between 465-630°C with a peak at 535.18°C, indicated the loss of **C_7H_7O** with an estimated mass loss of 20.88% (calculated = 21.36%). The final step, between 630–800°C with a peak at 655.31°C, related to the loss of **$C_3H_4N_2$** with an estimated mass loss of 12.91% (calculated = 13.58%). After complete decomposition, Cobalt oxide **(CoO)** remained as residues. The thermal decomposition analysis of the **$[Cu(HYD)Cl_2(H_2O)_2] \cdot H_2O$** complex occurred in three steps. The first step between 25-105°C with a peak at 90°C involved the loss of water molecules, resulting in a mass loss of 3.422%(calculated = 3.83%). The second step between 105-325°C with a peak at (135 and 299) °C included the loss of **$C_3H_{13}ClO_2$** and an estimated mass loss of 24.18%(calculated = 24.86%). The final step between 325-800°C with a peak at 611°C related to the loss of **$C_{14}H_{10}ClN_3$** with an estimated mass loss of 53.860%(calculated = 54.42%). Upon complete decomposition, copper oxide (**CuO**) remained as residue.

3.1.6. Geometry optimization.

3.1.6.1. DFT calculations for the (HYD) and its Cu (II) complex.

The initial structural models for the computational studies were based on the insights derived from spectroscopic analyses, including infrared (IR), ultraviolet-visible (UV-Vis), and Mass spectroscopy. These initial structures were optimized using density functional theory (DFT) calculations in the gas phase. The optimization process involved successive tightening of convergence criteria at each significant step until the minimum energy structures were obtained [59]. The optimized geometries of the (**HYD**) and its Cu(II) complex are depicted in Figure 3. The critical geometric parameters, such as bond lengths and angles, obtained from these optimization calculations are tabulated in Table 5. An analysis of this data revealed the following observations:

1. Upon complexation with the Cu(II) ion, an elongation of the coordination bonds was observed, with significant variations in bond lengths such as N(8)-N(9), N(9)-C(10), C(10)-C(11), C(11)-N(12) and N(12)-C(13)of the ligand (**HYD**) moiety. These bonds became slightly longer after complexation, confirming that coordination occurred via the two azo nitrogen atoms [60]. This elongation can be attributed to the redistribution of electron density upon forming coordination bonds between the metal ion and the nitrogen donors.
2. All active groups involved in the coordination with the Cu(II) ion, including the two azo nitrogen atoms, exhibited longer bond lengths compared to the free ligand (**HYD**) [61]. This observation is consistent with the formation of coordinate covalent bonds between the metal ion and the donor atoms of the ligand.
3. The bond angles within the free (**HYD**) ligand moiety underwent alterations upon coordination with the Cu(II) ion. Furthermore, the bond angles surrounding the central copper atom in the complex were found to be within the reported range for an octahedral geometry [62], suggesting a distorted octahedral coordination environment around the metal center.
4. The decrease in metal-chloride bond angles compared to the ideal octahedral geometry may be attributed to intramolecular hydrogen bonding interactions [60]. These hydrogen bonding interactions can influence the complex's geometry and bond angles.

The computational studies, supported by spectroscopic data, provided valuable insights into the structural features and bonding interactions within the (**HYD**) and its Cu(II) complex. These insights are crucial for understanding these metal-organic compounds' structure-property relationships and potential applications.

Table 5. Selected bond lengths and angles of minimum energy structures of the (**HYD**) and its Copper complex.

Bonds	Bond Lengths(Å)		Bonds	Bond Angles (°)
	(HYD)	Cu (II) Complex		Cu (II) Complex
N(8)-N(9)	1.336	1.345	Cl(26)-Cu(22)-Cl(25)	95.884
N(9)-C(10)	1.292	1.314	Cl(26)-Cu(22)-O(24)	132.698
C(10)-C(11)	1.461	1.462	Cl(26)-Cu(22)-O(23)	169.622
C(11)-N(12)	1.292	1.314	Cl(26)-Cu(22)-N(12)	88.926
N(12)-C(13)	1.402	1.429	Cl(26)-Cu(22)-N(9)	91.228
			Cl(25)-Cu(22)-O(24)	57.593
			Cl(25)-Cu(22)-O(23)	89.461
			Cl(25)-Cu(22)-N(12)	156.286
			Cl(25)-Cu(22)-N(9)	126.96
			O(24)-Cu(22)-O(23)	44.633
			O(24)-Cu(22)-N(12)	131.83
			O(24)-Cu(22)-N(9)	79.641
			O(23)-Cu(22)-N(12)	89.725
			O(23)-Cu(22)-N(9)	78.466
			N(12)-Cu(22)-N(9)	75.943

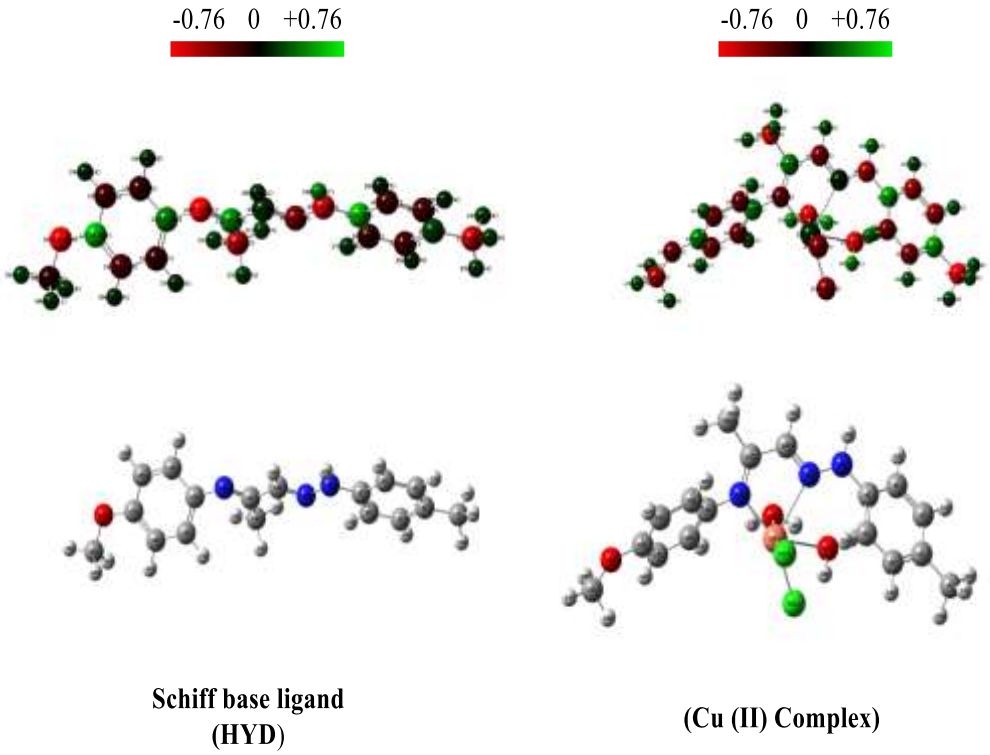

Fig 3. Geometrical Optimization structures of the (**HYD**) and its Cu (II) complex and atomic charge distributions are shown in color range.

3.1.6.2. Frontier molecular orbital analysis.

The highest occupied molecular orbital (HOMO) and lowest unoccupied molecular orbital (LUMO) were analyzed to gain insights into the electronic properties, chemical stability, and reactivity of the studied molecules [63]. The HOMO represents the ability of a molecule to donate an electron, while the LUMO characterizes its ability to accept an electron [64]. The energy gap between the HOMO and LUMO orbitals (HOMO-LUMO gap) provides valuable information about various molecular properties, such as kinetic stability, chemical reactivity, polarizability, and hardness. These properties for the different chemical species are compiled in Table 6. The calculated molecular orbitals (HOMO and LUMO) of the proposed model for the ligand and its copper complex are shown in Figure 4. Visualization of the frontier molecular orbitals (FMOs) reveals that the highest occupied molecular orbitals (HOMOs) are primarily localized on the phenol ring and azomethine group of the ligand. In contrast, the lowest unoccupied molecular orbitals (LUMOs) are predominantly centered on the copper metal ion [65]. This orbital distribution suggests that the azomethine functional group of the ligand participates in electron donation during complex formation [66]. This mechanistic rationale is further supported by the Mulliken and Hirshfeld charge analysis that was presented subsequently. Examining the frontier molecular orbitals shows that the copper complex's HOMO-LUMO gap (ΔE) is reduced by approximately 0.4022 eV compared to the corresponding gap in the free ligand. This decrease in the HOMO-LUMO gap implies the likelihood of $\pi \rightarrow \pi^*$ electron transitions between the HOMO and LUMO, as well as facile ligand-to-metal charge transfer processes [67]. These predictions align with the experimental electronic
spectra, where intense peaks attributable to these electronic transitions are distinctly observed for the complex. The analysis of the frontier molecular orbitals provides valuable insights into the electronic structure and reactivity of the studied compounds. The localization of the HOMO on the azomethine group supports its role as an electron donor during coordination with the metal ion. Furthermore, the reduced HOMO-LUMO gap in the metal complex suggests increased reactivity and the possibility of charge transfer processes, which can have implications for various applications, such as catalysis, optoelectronic devices, and biological activities.

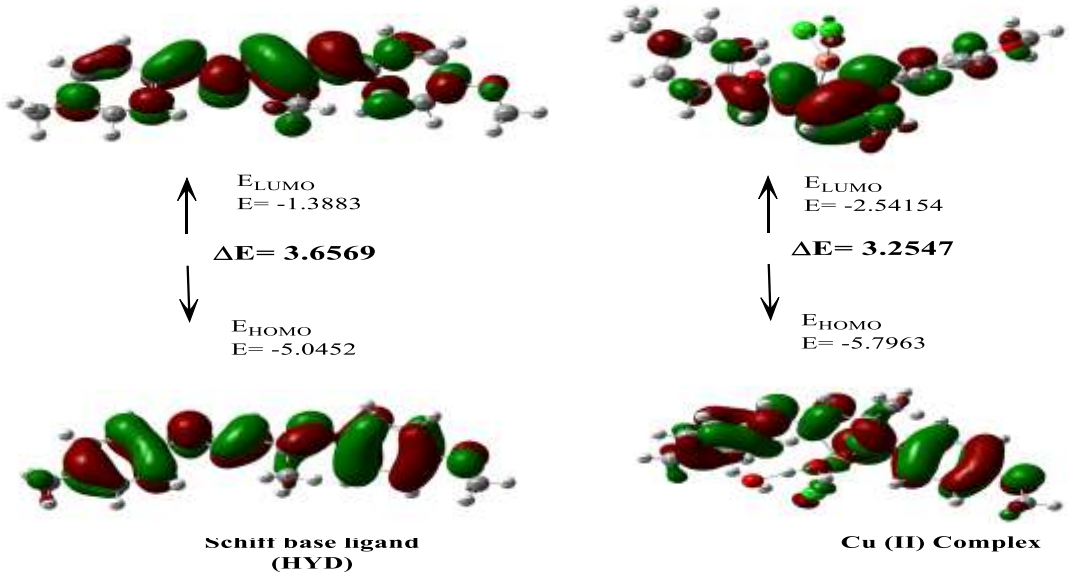

Fig 4. The HOMO-LUMO orbitals occupy the calculated energy gap.

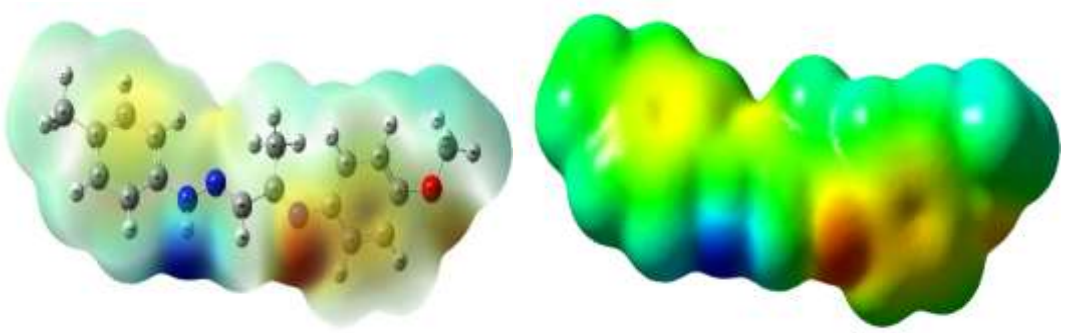

(A)

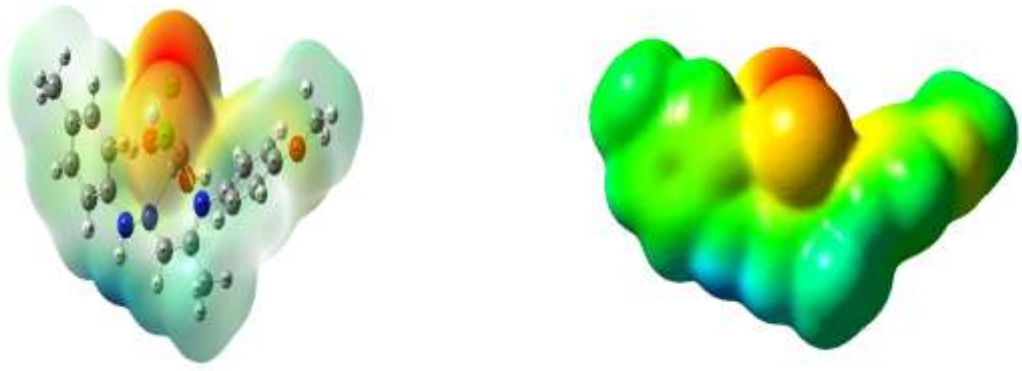

(B)

Fig 5. Molecular electrostatic potential (MEP) of **A)** Hydrazono Schiff base (**HYD**) and **B)** Cu (II) complex

Table 6. HOMO-LUMO gap (ΔE) ionization energies (IE), electron affinities (EA), hardness, chemical potential, and electrophilicity of the Hydrazono Schiff base (**HYD**) and its Cu (II) complex in the gas phase.

Compounds	ΔE (eV)	EA ($-E_{LUMO}$)	IE ($-E_{HOMO}$)	Chemical potential (Pi)	Hardness (η)	Electrophilicity (ω)
(HYD)	3.6569	-1.3883	-5.0452	-3.2167	1.8284	2.8296
Cu(II) Complex	3.2547	-2.54154	-5.7963	-4.16892	1.6273	5.3398

3.1.7. Bioactivity Screening

3.1.7.1. Antimicrobial Efficacies

Researchers recently investigated the antibacterial and antifungal properties of the (**HYD**)and its metal complexes with cobalt and copper. They used the disc diffusion method to evaluate these properties against various microorganisms [44, 53]. The study assessed the impact including gram-negative bacteria (*Escherichia coli and Salmonella enterica*), gram-positive bacteria (*Staphylococcus aureus and Streptococcus mutans*), and fungi (*Candida albicans and Aspergillus niger*). The antimicrobial activity is compared with standard antibiotics, such as gentamicin (for gram-negative bacteria), ampicillin (for gram-positive bacteria), and nystatin (for fungi). Overall, this study explored the antimicrobial properties of the metal complexes using disc diffusion testing. It provided evidence that these complexes can inhibit the growth of diverse bacteria and fungi [71-74]. The data is presented as the diameter of the zone of inhibition (in mm) with standard deviations, a common measure of antimicrobial activity in disc diffusion assays. Higher values indicate stronger antimicrobial activity. Compared to the free (**HYD**), the enhanced antibacterial efficacy observed in its metal complexes could be related to the chelation process, where the (**HYD**) coordinates with metal ions, endowing the resulting metal chelates with polar and nonpolar properties [75]. This property is advantageous as it facilitates the penetration of these complexes into cells and tissues. The diminished metal ion polarity results notably from the overlap of ligand orbitals during chelation, enabling a partial distribution of the positive charge of the metal ion among the coordinating donor groups. Consequently, chelation induces heightened π-electron delocalization across the entire chelate ring, thereby enhancing the permeability of the complexes through lipid membranes [76, 77]. Additionally, chelation processes augment the hydrophilic and lipophilic characteristics of central metal ions, potentially amplifying their lipid-soluble properties and facilitating their penetration through the lipid bilayer of cellular membranes. The coordination also alters lipophilicity, influencing the rate at which molecules enter cells. Consequently, the modified nature of the metal complex, as a result of coordination, renders it more active than the free Schiff base ligand [76, 78]. Upon analyzing the biological effects of the Hydrazono Schiff base (**HYD**), its cobalt(II) and copper(II) complexes, and standard drugs, a notable observation emerges: all the complexes exhibit superior inhibitory effects on bacterial and fungal growth compared to the original ligand. Several insights can be drawn from the antimicrobial test results (Table 7):

1. The complexes' observed antibacterial efficacy is attributed to the imine moieties (-C=N) within them. It is suggested that their mechanism of action involves the creation of hydrogen bonds via the (C=O) azomethine group, which interacts with vital cellular components. This interaction may disrupt normal cellular processes, contributing to the compounds' antibacterial properties.
2. Chelation with metal ions results in decreased polarity as the positive charge of the metal ion is neutralized by the ligand-donor groups. This process enhances the hydrophobic and lipophilic nature of the ligands, facilitating their permeation through the lipid layers of cell membranes. This penetration can lead to the deactivation of enzymes involved in cellular respiration and the inhibition of protein synthesis, effectively restricting the growth of the organisms.
3. The data suggests that the copper complex exhibits higher toxicity against bacterial species and fungi than the Schiff base ligand and cobalt complex, showing significant potential as an antimicrobial agent.
4. In terms of antifungal activity against *Candida albicans*, the compounds' effectiveness ranks in the following order: Cu(II) complex > Hydrazono Schiff base (**HYD**) > Co(II) complex. Against *Aspergillus niger*, the order is Cu(II) complex > Co(II) complex > Hydrazono Schiff base (**HYD**).

These observations suggest that cobalt and copper complexes generally exhibited better antimicrobial activity than the Hydrazono Schiff base (**HYD**) alone, notably against gram-positive bacteria and fungi. The metal complexes showed promising antifungal activity and moderate to high activity against certain bacterial strains, indicating the potential of incorporating metal ions to enhance the biological activity of the Schiff base ligand [79].

Table 7. Exploring the Bioactivity of the (**HYD**)and Its Metal Complexes: An Investigation into Biological Effects

Sample / Microorganism	(HYD)	Co(II) Complex	Cu(II) Complex	Standard antibiotic
Gram-negative bacteria				Gentamicin
***Escherichia coli* (ATCC:10536)**	18.3±0.6	21.3±0.6	23.7±0.6	27.0±1.0
***Salmonella enterica* (ATCC: 14028)**	9.0±1.0	11.0±1.0	16.0±1.0	18.3±0.6
Gram-positive bacteria				Ampicillin
***Staphylococcus aureus* (ATCC:13565)**	7.0±1.0	19.4±0.6	17.7±0.6	22.0±1.0
***Streptococcus mutans* (ATCC:25175)**	21.3±0.6	22.9±0.6	31.7±0.6	20.3±0.6
Fungi				Nystatin
***Candida albicans* (ATCC:10231)**	22.7±0.6	18.3±0.6	26.3±0.6	21.0±1.0
***Aspergillus Nigar* (ATCC:16404)**	22.3±0.6	23.8±1.0	31.0±1.0	19.3±0.6

3.1.8. Docking study

The (**HYD**)and its Cu (II) complex were exposed to computational molecular docking analysis using the Molecular Operating Environment (MOE, version 2014.10) software [80]. This analysis was performed in conjunction with IXA bound to tubulin (PDB ID: 7DAF) as the receptor. All structural optimizations were conducted within MOE until reaching a root mean square deviation (RMSD) gradient of 0.05 kcal mol^{-1} $Å^{-1}$ using the MMFF94x force field, and the partial charges were automatically assigned. The subsequent receptor, with **PDB ID: 7DAF**, displays the crystal structure of three compounds known for stabilizing microtubules in complex with tubulin. This structure offers insights into the development of novel drugs. Microtubules are crucial cytoskeleton components recognized as significant targets in cancer therapy. In particular, inhibitors that target the taxane-binding site on tubulin, such as taxol analogs and epothilones, have demonstrated considerable efficacy in clinical trials, representing promising avenues for cancer treatment [81,104]. In experimental observations, the Hydrazono Schiff base (**HYD**) demonstrated a noteworthy IC_{50} value of 372.99 µg/ml when assessed against a breast cancer cell line. Furthermore, the Copper (II) complex is denoted as **$[Cu(HYD)Cl_2(H_2O)_2].H_2O$**, derived from the ligand mentioned above, exhibited enhanced anticancer efficacy, displaying reduced IC_{50} values of 322.80 µg/ml. To validate these findings, theoretical docking studies focused on the (**PDB ID: 7DAF**), a vital target for cancer therapy. Docking analysis outcomes using PDB ID: 7DAF indicated that both the Hydrazono Schiff base (**HYD**) and its Copper (II) complex, **$[Cu(HYD)Cl_2(H_2O)_2].H_2O$** displayed notably low binding energies of -0.6 and -18.1 kcal mol^{-1}, respectively. This implies heightened activity in the complexes compared to the original ligand, owing to the establishment of coordination bonds with the Copper (II) metal ion. The results of docking simulations for Hydrazono Schiff base (**HYD**)and its Copper (II) complex are depicted through both two-dimensional (2D) and three-dimensional (3D) representations, as presented in Fig 6. Furthermore, Table 8 elucidates the binding energies associated with the Hydrazono Schiff base (**HYD**) and its Copper (II) complex.

Table 8. Results of docking interactions to IXA bound to tubulin in cancer cell with Hydrazono Schiff base (**HYD**) and its Cu (II) complex

Cancer cell Receptor	Cpds	Ligand moiety	Receptor site	Interaction	Distance (Aº)	E (kcal/mol)
7DAF	**(HYD)**	6-ring	CB ALA 12 (A)	pi-H	3.54	-0.6
		6-ring	6-ring TYR 224 (A)	pi-pi	4.00	-0.0
	Cu complex	N 8	OD1 ASP 98 (A)	H-donor	3.32	-1.5
		O 26	OD2 ASP 98 (A)	H-donor	2.82	-18.1
		C 12	N GLY 144 (A)	H-acceptor	4.12	-1.6
		O 25	OE1 GLU 71 (A)	ionic	3.72	-1.1
		O 25	OD2 ASP 98 (A)	ionic	2.73	-6.6
		O 26	OE1 GLU 71 (A)	ionic	3.75	-1.1
		O 26	OD2 ASP 98 (A)	ionic	2.82	-5.8

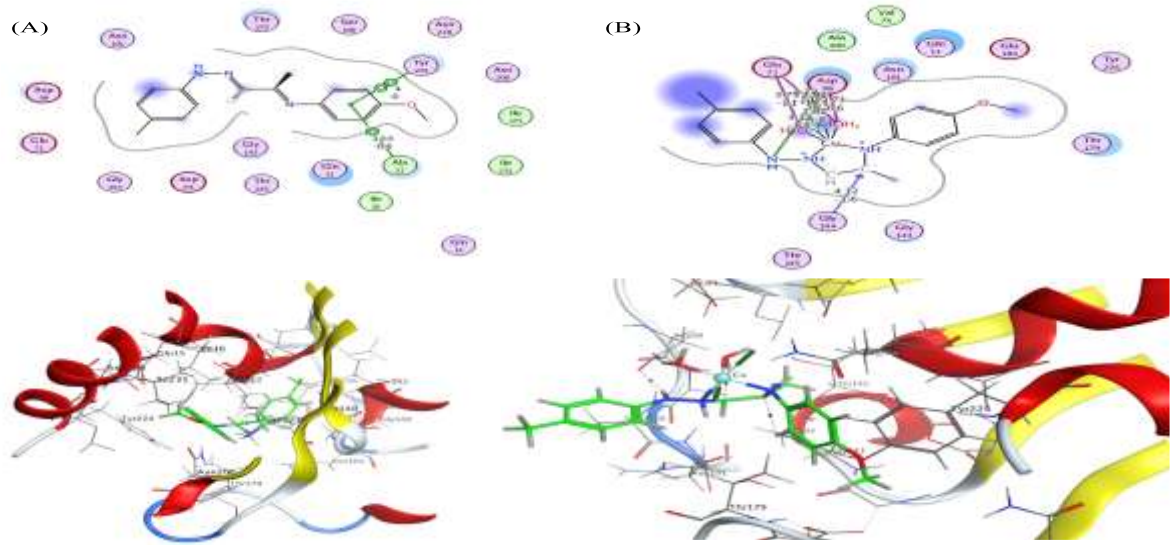

Fig 6. Visual Representation of Breast Cancer Receptor (**PDB:7DAF**) Interaction with **(A)** Hydrazono Schiff base (**HYD**) and **(B)** its Cu (II) Complex: Comparative 2D & 3D Diagrams.

3.2. Characterization of Nano Hydrazono Copper Complex.

3.2.1. XRD

Recent advancements in powder X-ray diffraction (XRD) methodologies have significantly improved the analytical abilities of mineralogists and solid-state chemists in investigating the physicochemical composition of unknown materials [82, 83]. XRD remains an extensively used technique for revealing the dimensions and geometric qualities of the unit cell in diverse compounds, providing crucial qualitative, quantitative, and multifaceted analytical perspectives. Examining peak positions within the X-ray diffraction (XRD) pattern elucidates the translational symmetry and unit cell characteristics. Specifically, recognizing distinct Bragg reflections at 2θ values of 32.158°, 45.932 °, 75.844 °, 56.987 °, and 29.002 ° helps reveal the dimensions and geometry of the unit cell. These reflections correspond to the (111), (211), (220), (200), and (110) crystallographic planes, respectively, indicating the face-centered cubic arrangement inherent in metallic copper. as shown in Figure (7).

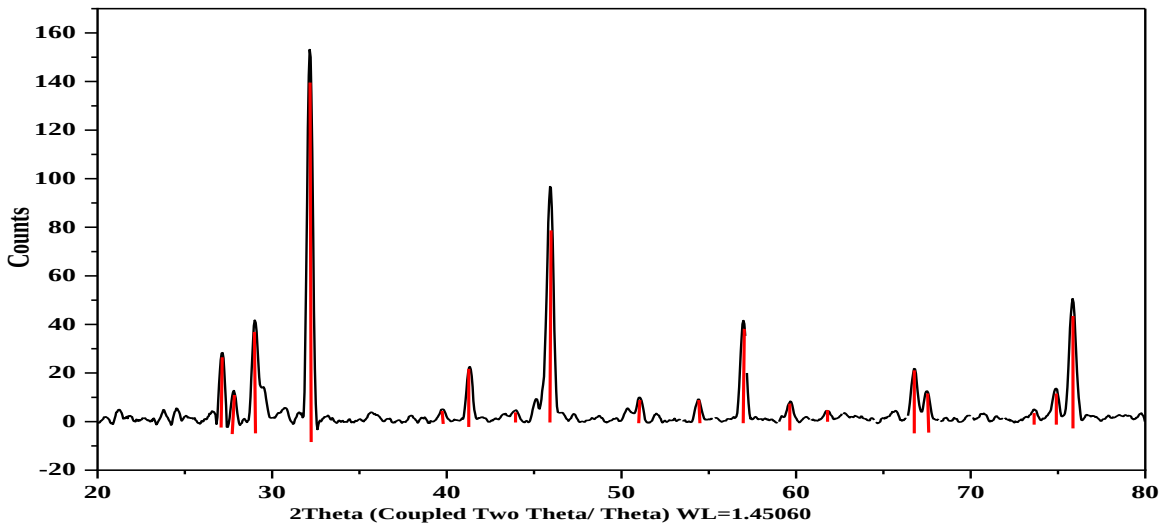

Fig 7. Material Composition Analysis in the Newly Synthesized Nano Hydrazono Copper Complex Using Powder X-ray Diffraction Methods.

3.2.2. Textural Characters SEM of Hydrazono Copper Complex Nanoparticles

Recent examinations have employed scanning electron microscopy (SEM) to investigate the dispersion properties of nanoparticles derived from the Hydrazono copper complex. The SEM images revealed a notable degree of homogeneity among the fabricated particles, depicting individual entities with spherical porous morphology and a lack of apparent aggregation or agglomeration [84]. Furthermore, the measured diameters of these nanoparticles were observed to be below 100 nm, as shown in Figure 8.

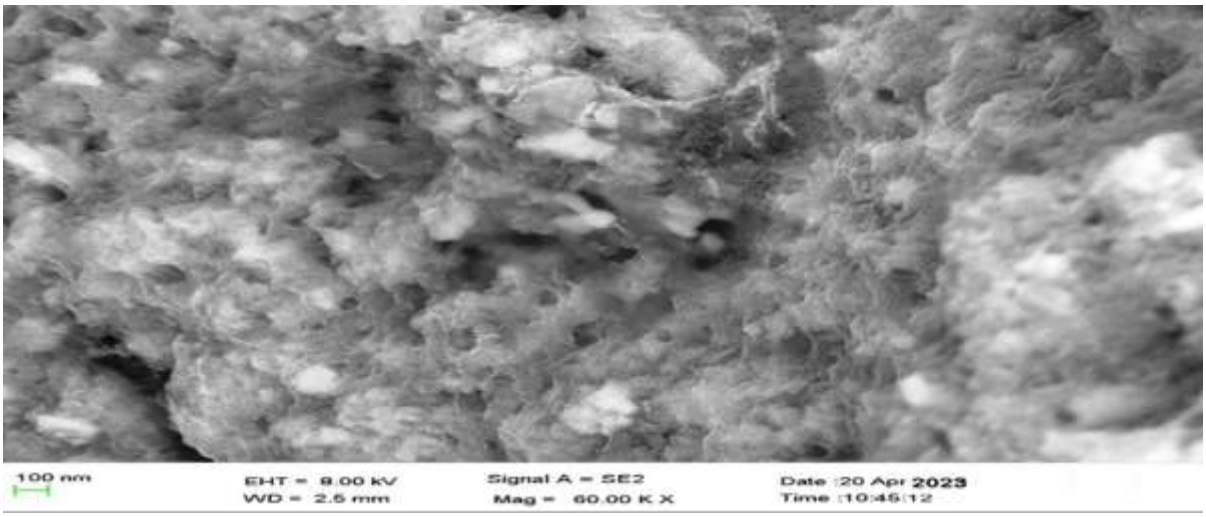

Fig 8. Scanning Electron Microscopy Analysis of Hydrazono Copper Complex Nanoparticles

3.2.3. Textural Characters (AFM) of Hydrazono Copper Complex Nanoparticles.

An atomic force microscope (AFM) was used to examine the surface attributes of a recently produced Hydrazono nanocopper complex [85].AFM images clearly showed a porous fibrous morphology, as depicted in Figure 9. This porous fibrous structure indicated that the particles were not agglomerated or aggregated [86]. Examination of the AFM images allowed the researchers to quantify particle dimensions. Analysis revealed that the particles had a size of 88 nm.

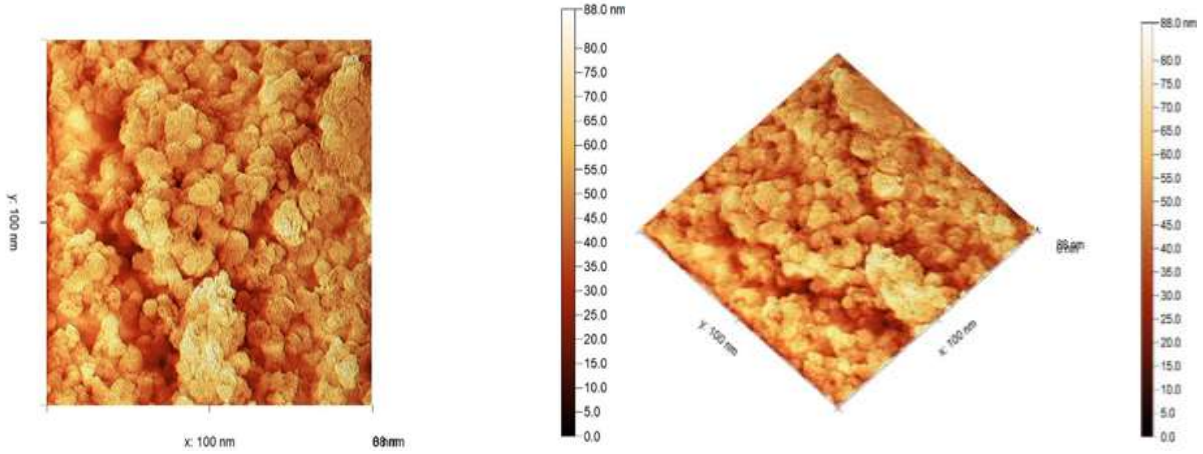

(A) **(B)**

Fig 9. Visualize **(A)** Two and **(B)** Three-Dimensional Atomic Force Microscopy of Hydrazono Copper Complex Nanoparticles Formed by Copper Complexes with Hydrazono Schiff Base

3.2.4. DLS and Zeta Potential

Recent work has utilized dynamic light scattering (DLS) to characterize the particle size of the Hydrazono nanocopper complex. DLS analysis of the Hydrazono nano copper complex revealed an average particle size of 43.8 nm, as shown in Figure 10. Further investigations found an unimodal size distribution with low polydispersity, indicating a uniform particle size [63]. Additionally, the system exhibited excellent colloidal stability. Insights into the stability of the nano copper complex were provided by examining the particle size distribution and zeta potential results. The zeta potential measurement of -24 mV signifies a well-dispersed system and underscores the physicochemical stability, especially under storage. The higher zeta potential absolute values correspond to the stability [64]. Zeta potential is a pivotal parameter for assessing the physicochemical stability of nanoparticles during storage. In the case of the Hydrazono nano copper complex, the negative zeta potential of -24 mV confirms its enhanced stability, as illustrated in Figure 11.

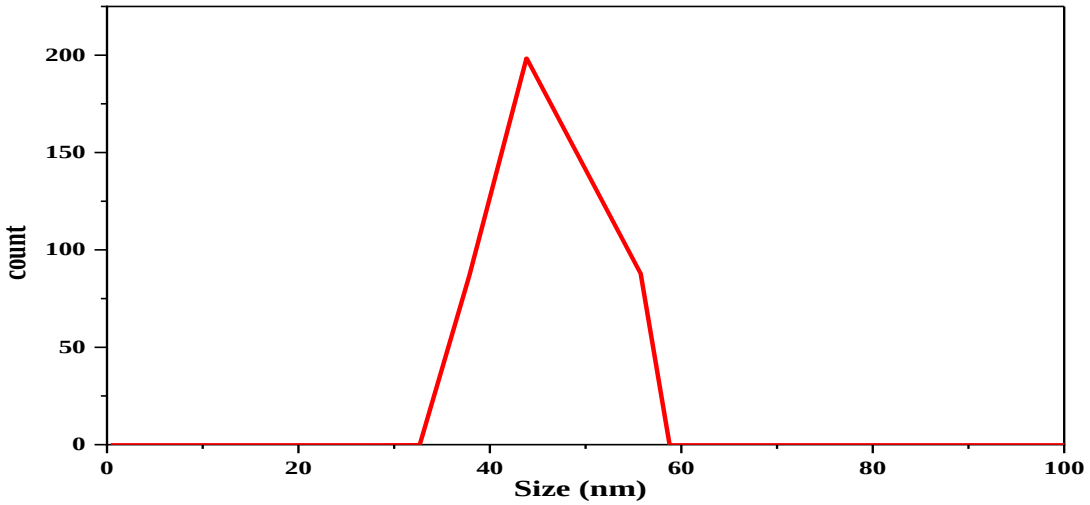

Fig 10. Particle Size Distribution Analysis of Hydrazono Nano Copper Complex by Dynamic Light Scattering (DLS)

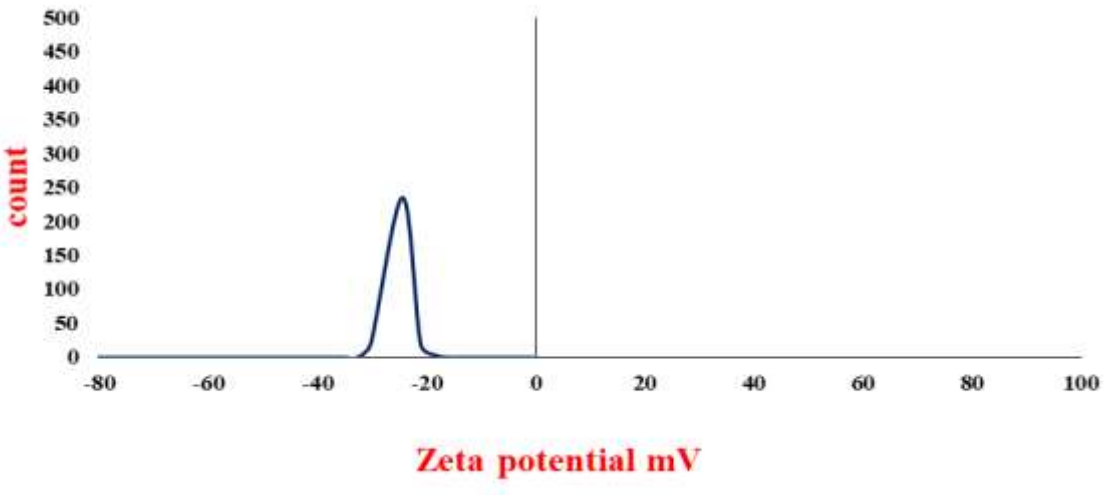

Fig 11. Zeta Potential Analysis Confirms Enhanced Stability of Hydrazono Nano Copper Complex (-24 mV)

3.2.5. BET surface area and pore size.

The Brunauer-Emmett-Teller (BET) methodology, named after its developers, is an invaluable technique for characterizing nanoscale materials. BET relies on the physical adsorption of gases onto solid surfaces, providing a rapid and straightforward means of determining surface area [89]. This approach was utilized to analyze the surface area properties of a nanocopper complex. BET adsorption isotherms were crucial in scrutinizing the complex's surface area characteristics. De

Boer's classification proved useful for classifying isotherms depicting hysteresis loops, allowing for a meticulous examination of porous configurations [90]. Specifically, nitrogen adsorption-desorption isotherms consistently exhibited a Type IV pattern for all Hydrazono copper complex nanoparticle samples, confirming the presence of macropores. Multipoint BET surface area analysis determined a notable value of 35.0007 m^2/g, accompanied by an average pore size of 6.74532 nm and particle radius of 3.8960e+001nm. The substantial surface area elucidated by BET analysis (Figure 12) greatly enhances the nanoparticles' ability to adsorb cadmium ions in water. The macroporous structure stems from the spherical morphology, amplifying the

surface's affinity for cadmium adsorption. Crucially, this macroporous architecture plays a pivotal role in augmenting the efficacy of cadmium ion adsorption by the metal complex nanoparticles.

Table 9. Cytotoxicity Assessment of Hydrazono Nano Copper Complex: Viability, Toxicity, and IC_{50} Values

ID	Conc. ug/ml	O.D			Mean O.D	ST.E	Viability %	Toxicity %	IC_{50}
Cu(II)	10000	0.048	0.042	0.05	0.046667	0.002404	6.029285099	93.970714901	648.41
	5000	0.064	0.062	0.057	0.061	0.002082	7.881136951	92.118863049	
	2500	0.126	0.137	0.129	0.130667	0.003283	16.881998277	83.118001723	
	1250	0.262	0.262	0.255	0.259667	0.002333	33.548664944	66.451335056	
	625	0.396	0.397	0.394	0.395667	0.000882	51.119724376	48.880275624	
	312.5	0.487	0.498	0.486	0.490333	0.003844	63.350559862	36.649440138	
	156.25	0.65	0.643	0.645	0.646	0.002082	83.462532300	16.537467700	
	78.12	0.765	0.761	0.769	0.765	0.002309	98.837209302	1.162790698	

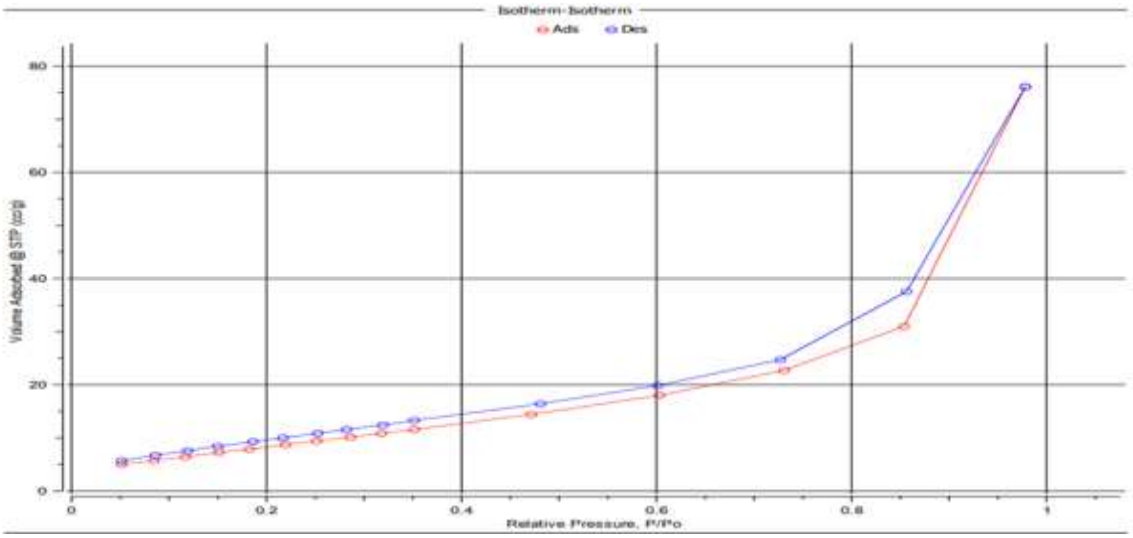

Fig 12. Surface Characteristics and Adsorption Capacities of Nanostructured Hydrazono Copper Complex via BET Analysis.

3.2.6. Contact angle, Hydrophobicity, and toxicity of Hydrazono Copper Nano complex

The Hydrazono Nano copper complex particles exhibited a hydrophobic nature, as evidenced by a water contact angle of 126° (Fig 13. B). This significant hydrophobicity in water greatly enhances the effectiveness of these nanoparticles as sensors in aqueous environments [91, 92]. To develop an environmentally friendly Nano particle-based sensor, it is crucial to utilize non-toxic materials. The cytotoxicity of the Hydrazono Nano copper complex was assessed, revealing an IC_{50} value of 648.41 µg/ml (Table 9). This high IC_{50} value indicates that the Nano copper complex has low toxicity (Fig 13. A), further supporting its suitability as a sensor in water environments [93, 94].

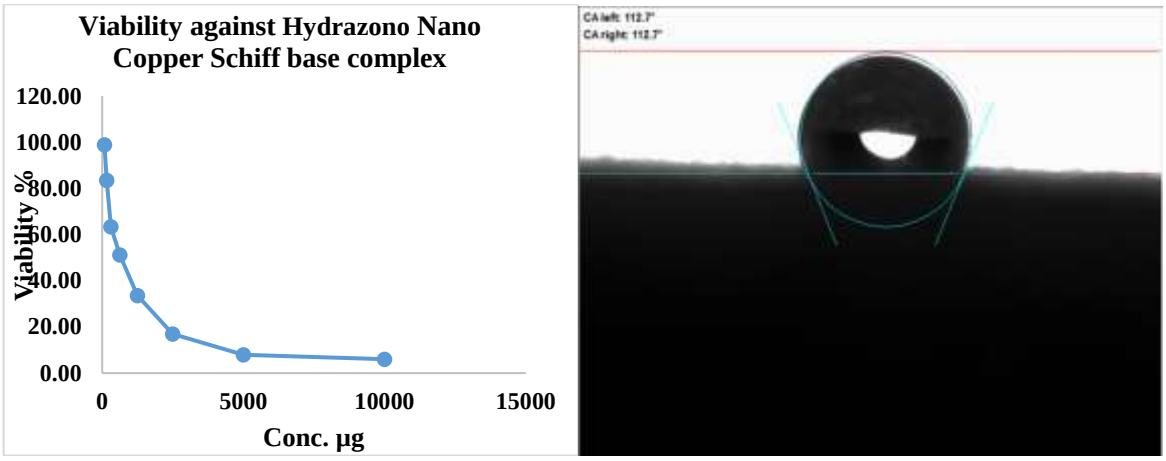

(A) **(B)**

Fig 13. **(A)** Non-Toxic and **(B)** Hydrophobic Properties of Hydrazono Nano Copper Complex Particles

3.2.7. Real-time Detection of Cadmium Ion Contamination Using a Nano Copper Schiff Base Complex-modified Quartz Crystal Microbalance Sensor

The QCM (Quartz Crystal Microbalance) technique, when combined with Hydrazono nano copper complex as the sensing material, can be used to detect cadmium ion contamination. Here's a general overview of how this sensor technique works [95, 96]:

1. **Quartz Crystal Microbalance (QCM) principle:**
   - The QCM comprises a thin quartz crystal disc coated with electrodes on both sides.
   - When an alternating electric field is applied across the electrodes, the quartz crystal oscillates at a specific resonant frequency, which is highly sensitive to changes in mass on its surface.
2. **Sensor fabrication:**
   - The Hydrazono Nano copper complex is immobilized or coated on the surface of the quartz crystal.
   - This Hydrazono Nano copper complex acts as the sensing material and has a high affinity for binding with cadmium ions.
3. **Sensing mechanism:**
   - When the QCM sensor is exposed to an environment containing cadmium ions, the Nano copper Schiff base complex on the crystal surface interacts and binds with the cadmium ions.
   - This binding event leads to a change in the mass on the quartz crystal surface, which alters the resonant frequency of the crystal.
4. **Frequency measurement:**
   - The QCM measures the change in the resonant frequency of the quartz crystal before and after exposure to the cadmium ion-containing environment.
   - This frequency shift is directly proportional to the mass change on the crystal surface, which is caused by the binding of cadmium ions to the Nano copper Schiff base complex.
5. **Quantification:**
   - By calibrating the QCM sensor with known concentrations of cadmium ions, a correlation can be established between the observed frequency shift and the concentration of cadmium ions in the sample.
   - This allows for quantitatively measuring cadmium ion contamination levels based on the observed frequency shift.

The advantages of using the QCM technique with Hydrazono Nanocopper Schiff base complex include high sensitivity, real-time monitoring capabilities, and the potential for miniaturization and portability. Additionally, the Hydrazono Nano copper complex can be tailored to enhance its selectivity towards cadmium ions, minimizing interference from other ions or compounds. It's important to note that practical implementation may involve additional steps, such as surface modification, Hydrazono Nano copper complex synthesis optimization, and data analysis techniques, to ensure accurate and reliable detection of cadmium ion contamination.

3.2.8. **Novel Sensing Mechanism for Nano Copper Complex on Quartz Crystal Microbalance (QCM)**

The interaction between cadmium ions and the Hydrazono Nano copper complex sensor is governed by several types of intermolecular forces and interactions, including [97]:

1. Dipole-dipole interactions: Cadmium ions, being less electronegative, exhibit an asymmetric sharing of electrons with the Hydrazono Nano copper sensor. This asymmetry results in the formation of dipole moments, leading to the alignment of the electron clouds and dipole-dipole interactions between the two entities.

2. Donor-acceptor interactions: The Hydrazono Nano copper complex possesses polar side chains that act as electron donors. These side chains contribute to an increased negative charge density on the complex's surface, making it more prone to interact with cadmium ions through electrostatic attractions.
3. π-π interactions: The Hydrazono Nano copper complex likely contains aromatic or conjugated systems that can participate in π-π interactions with the cadmium ions. These interactions involve overlapping π-orbitals, further enhancing the binding between the two species.
4. Electrostatic attractions: Due to the negative charge density on the Hydrazono Nano copper complex surface and the positive charge of cadmium ions, electrostatic attractions also play a role in the binding process.

The intricate interplay of these interaction mechanisms, including dipole-dipole interactions, π-π interactions, donor-acceptor interactions, and electrostatic attractions, contributes to the overall binding phenomenon between cadmium ions and the Hydrazono Nano copper complex sensor. This comprehensive interaction profile, involving multiple types of intermolecular forces and interactions, provides a deeper understanding of the complex binding process and the factors that influence the sensitivity and selectivity of the sensor towards cadmium ions.

3.2.9. Effect of pH on Sensor Functionality

A. At pH 11 (red curve):

The sensor exhibits the highest initial sensitivity, as indicated by the sharp and substantial decrease in the parameter (frequency or mass change) at the beginning of the curve (Fig 14). This high initial sensitivity can be attributed to the deprotonated state of the Hydrazono Schiff base copper complex, facilitating strong initial interactions with cadmium ions. However, the high sensitivity is short-lived, and the curve flattens out relatively quickly, suggesting a reduced sensitivity over time at this pH. This behavior can be explained by the competitive effect of sodium ions (Na^+) present in the solution due to pH adjustments [98, 99]. At pH 11, the concentration of sodium ions is higher, and they compete with cadmium ions for the available binding sites on the surface of the Hydrazono Nano copper complex sensor. This competition hinders the adsorption of cadmium ions onto the sensor material, leading to a decrease in sensitivity over time, as observed in the flattening of the red curve [100-104].

B. At pH 7 (purple curve):

The initial decrease in the parameter is less pronounced compared to pH 11, indicating a lower initial sensitivity. However, the curve gradually decreases for a longer period, suggesting that the sensor retains its sensitivity for a longer duration at this pH. The lower concentration of sodium ions at pH 7 reduces the competition for binding sites, allowing for better adsorption and sustained sensitivity towards cadmium ions.

C. At pH 3.5 (green curve):

The sensor exhibits the lowest initial sensitivity, as evident from the smallest change in the parameter at the beginning of the curve. However, the curve maintains a consistent and gradual decrease over time, indicating sustained sensitivity at this pH. At this lower pH, the protonation state of the Schiff base ligand and the copper complex may hinder their initial interactions with cadmium ions, leading to lower initial sensitivity. Additionally, the concentration of sodium ions is minimal, minimizing the competitive effect and allowing for more favorable adsorption of cadmium ions onto the sensor surface over time. In comparison, Komyha et al. (2024) evaluated their sensor's performance at pH levels of 4, 7, and 11 for cadmium ion detection. They reported that maximum adsorption and sensitivity occurred at pH 4-6, significantly decreasing at higher pH levels due to cadmium ions precipitating as hydroxides and competing Na^+ ions reducing the adsorption efficiency [105]. These findings highlight the importance of pH in determining sensor performance, with both studies showing optimal sensitivity within specific pH ranges and diminished performance at extreme pH levels.

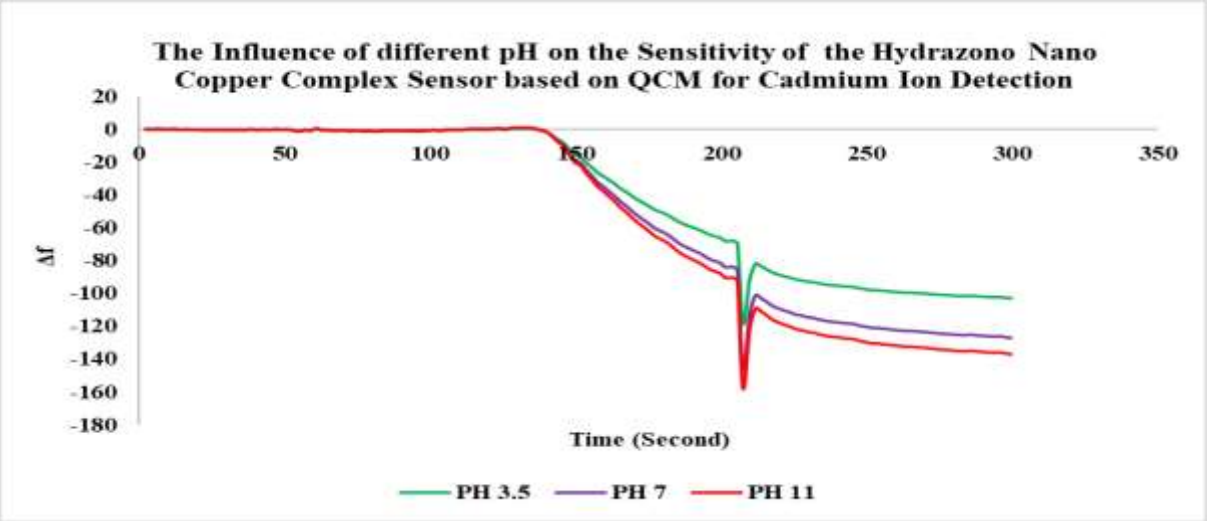

Fig 14. Impact of pH Variation on Performance of Hydrazono Nano Copper Complex QCM Sensor (Green: pH 3.5, purple: pH 7, Red: pH 11)

3.2.10. Effect of Temperature

The graph illustrates (Fig 15) the influence of different temperatures (20°C, 25°C, and 30°C) on the sensitivity of a Schiff base copper nanocomplex sensor based on the Quartz Crystal Microbalance (QCM) technique for cadmium ion detection.

A. At 20°C (blue curve):

The sensor exhibits the lowest initial sensitivity, as indicated by the smallest change in the parameter (frequency or mass change) at the beginning of the curve. However, the curve maintains a gradual and consistent decrease over time, suggesting sustained sensitivity at this temperature.

B. At 25°C (red curve):

The sensor shows the highest initial sensitivity, as evident from the sharp and substantial decrease in the parameter at the curve's start. This high initial sensitivity indicates favorable interactions between the sensor surface and cadmium ions at this temperature. However, the sensitivity decreases rapidly over time, as seen by the curve's flattening.

C. At 30°C (green curve):

The initial sensitivity is moderate, falling between the 20°C and 25°C curves. The curve gradually decreases, indicating sustained sensitivity over time, but not as consistently as the 20°C curve. The observed differences in sensitivity can be attributed to the relationship between the surface area of the Schiff base copper nanocomplex and the amount of adsorption of cadmium ions [100-104]. At lower temperatures (20°C), the surface area of the nanocomplex may be more restricted, limiting the initial adsorption of cadmium ions and resulting in lower initial sensitivity. However, as time progresses, the gradual decrease in the curve suggests that cadmium ions continue to adsorb onto the available surface area, leading to sustained sensitivity. At higher temperatures (25°C), the increased thermal energy could lead to enhanced surface area and exposure of more active sites on the Hydrazono copper nanocomplex. This increased surface area facilitates better initial adsorption of cadmium ions, resulting in high initial sensitivity. However, over time, the rapid flattening of the curve may be due to factors such as saturation of available binding sites or changes in the surface properties of the nanocomplex, leading to reduced sensitivity. At an intermediate temperature (30°C), the surface area and adsorption properties of the nanocomplex are balanced, resulting in moderate initial sensitivity. The gradual decrease in the curve suggests sustained adsorption of cadmium ions over time, but not as consistently as at 20°C, potentially due to competing effects of increased surface area and thermal factors. In summary, temperature plays a crucial role in the sensitivity of the Hydrazono copper nanocomplex sensor toward cadmium ion detection. The surface area of the nanocomplex, which is influenced by temperature, affects the initial adsorption and subsequent adsorption behavior of cadmium ions. Optimizing the temperature can ensure high initial and sustained sensitivity over time, depending on the application's specific requirements. Our findings indicated that the sensor's sensitivity was significantly influenced by temperature, with optimal performance observed at lower temperatures. This is consistent with the study conducted by Komyha et al. (2024) on cadmium ion detection using a nano cobalt complex QCM sensor. It similarly investigated temperature variations and found that the sensor's sensitivity decreased at higher temperatures due to increased molecular diffusion and the potential cleavage of chemical bonds on the sensor surface, leading to reduced performance [105]. This study underscores the critical role of temperature in modulating sensor performance, revealing that elevated temperatures negatively impact sensitivity through similar mechanisms.

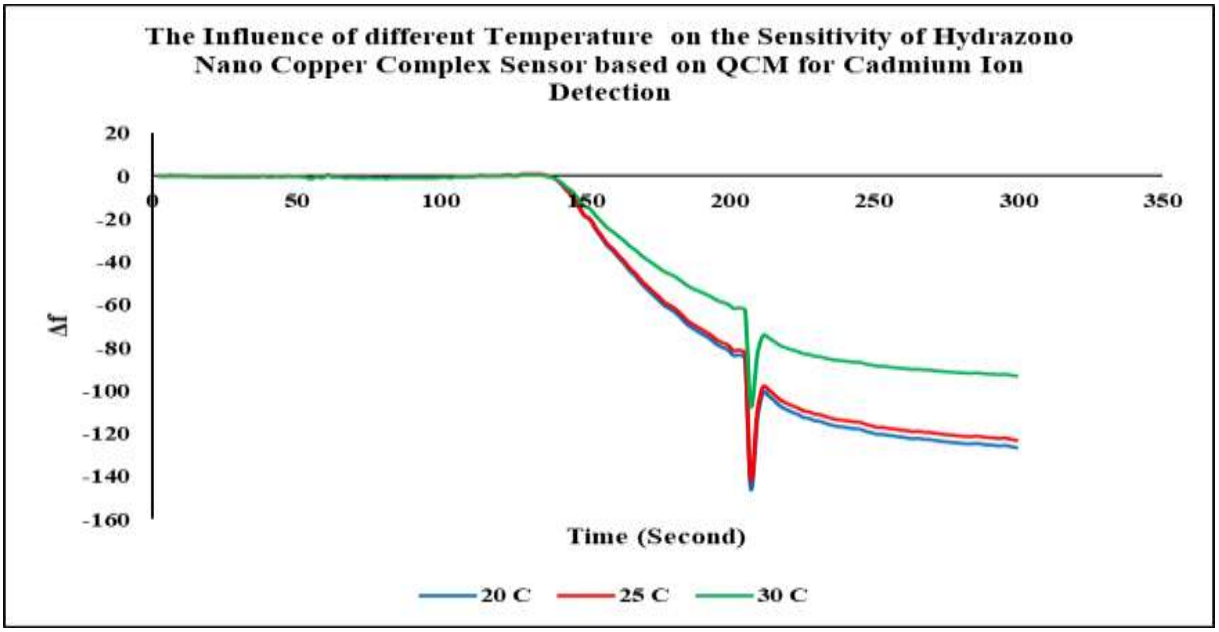

Fig 15. Influence of Temperature on Cadmium Ion Detection Sensitivity

IV. Conclusion

This study presents the development and characterization of nanoscale Schiff base ligand (HYD) and its metal complexes with cobalt (II) and copper (II) ions, highlighting their enhanced antimicrobial properties and their application in heavy metal detection. Advanced analytical techniques such as XRD, SEM, AFM, FTIR, DLS, and TGA provided detailed insights into their structural and physicochemical properties. The antimicrobial efficacy of these complexes was tested against various bacterial and fungal strains, demonstrating that both cobalt and copper complexes exhibited superior inhibitory effects compared to the free Schiff base ligand (HYD). The copper complex, in particular, showed the highest antimicrobial activity, surpassing some standard antibiotics. The enhanced efficacy is attributed to the chelation process, which increases cell permeability by reducing metal ion polarity and enhancing hydrophilic and lipophilic properties. Computational modeling (DFT) and molecular docking simulations further elucidated the complexes' optimized structure and binding interactions. The sensitivity analysis using Quartz Crystal Microbalance (QCM) demonstrated the exceptional performance of the nanostructured Hydrazono copper (II) complex in detecting cadmium ions with a rapid response time. This indicates its potential for effectively monitoring and remedying cadmium contamination in water and soil ecosystems. Overall, this study underscores the significant potential of nanoscale Schiff base ligand (**HYD**) and its metal complexes as powerful antimicrobial agents and efficient sensors for heavy metal detection, offering promising applications in medical, environmental, and biosensing fields.

References

1. A. P. Mishra and M. Soni, “Synthesis, structural, and biological studies of some Schiff bases and their metal complexes,” Met. Drugs, vol. 2008, no. 1, p. 875410, 2008.
2. C. Boulechfar et al., “Schiff bases and their metal Complexes: A review on the history, synthesis, and applications,” Inorg. Chem. Commun., vol. 150, p. 110451, 2023.
3. M. I. Khan, S. Gul, and M. A. Khan, “Schiff bases and their metallic derivatives: highly versatile molecules with biological and abiological perspective,” in Stability and Applications of Coordination Compounds, IntechOpen, 2019.
4. R. Kumar et al., “Synthesis, antibacterial and antifungal activities of Schiff base rare earth metal complexes: a review of recent work,” J. Coord. Chem., vol. 76, no. 9–10, pp. 1065–1093, 2023.
5. P. Varma, “Synthesis and characterization of metal complexes with chelating ligands.” Department of Chemistry, University of Calicut, 2018., 2018.
6. S. A. Dalia et al., “A short review on chemistry of schiff base metal complexes and their catalytic application,” Int. J. Chem. Stud, vol. 6, no. 3, pp. 2859–2867, 2018.
7. A. Çukurovali, I. Yilmaz, H. Özmen, and M. Ahmedzade, “Cobalt (II), copper (II), nickel (II) and zinc (II) complexes of two novel Schiff base ligands and their antimicrobial activity,” Transit. Met. Chem., vol. 27, pp. 171–176, 2002.
8. J. Karges, R. W. Stokes, and S. M. Cohen, “Metal complexes for therapeutic applications,” Trends Chem., vol. 3, no. 7, pp. 523–534, 2021.
9. K. J. Franz and N. Metzler-Nolte, “Introduction: metals in medicine,” Chemical Reviews, vol. 119, no. 2. ACS Publications, pp. 727–729, 2019.
10. L. H. Abdel-Rahman, A. M. Abu-Dief, R. M. El-Khatib, and S. M. Abdel-Fatah, “Sonochemical synthesis, DNA binding, antimicrobial evaluation and in vitro anticancer activity of three new nano-sized Cu (II), Co (II) and Ni (II) chelates based on tri-dentate NOO imine ligands as precursors for metal oxides,” J. Photochem. Photobiol. B Biol., vol. 162, pp. 298–308, 2016.
11. D. Osman, A. Cooke, T. R. Young, E. Deery, N. J. Robinson, and M. J. Warren, “The requirement for cobalt in vitamin B12: A paradigm for protein metalation,” Biochim. Biophys. Acta (BBA)-Molecular Cell Res., vol. 1868, no. 1, p. 118896, 2021.
12. A. Frei et al., “Nontoxic Cobalt (III) Schiff Base Complexes with Broad-Spectrum Antifungal Activity,” Chem. Eur. J., vol. 27, no. 6, pp. 2021–2029, 2021.
13. J. Lv, T. Liu, S. Cai, X. Wang, L. Liu, and Y. Wang, “Synthesis, structure and biological activity of cobalt (II) and copper (II) complexes of valine-derived schiff bases,” J. Inorg. Biochem., vol. 100, no. 11, pp. 1888–1896, 2006.
14. R. Meena, P. Meena, A. Kumari, N. Sharma, and N. Fahmi, “Schiff Bases and Their Metal Complexes: Synthesis, Structural Characteristics and Applications,” in Schiff Base in Organic, Inorganic and Physical Chemistry, IntechOpen, 2023.
15. [1] M. Hasanzadeh Esfahani and M. Behzad, “Crystal structure and antibacterial properties of a new dinuclear copper complex based on an unsymmetrical NN′ O type Schiff base ligand,” J. Coord. Chem., vol. 73, no. 1, pp. 154–163, 2020.
16. B. Kaya, T. Karakurt, O. Şahin, and B. Ülküseven, “Four and six-coordinated cobalt complexes based on thiosemicarbazone. Formation, experimental and theoretical characterization,” J. Mol. Struct., vol. 1250, p. 131783, 2022.
17. T. Bhattacharjee et al., “Syntheses, crystal structures, theoretical studies, and anticancer properties of an unsymmetrical schiff base ligand N-2-(6-methylpyridyl)-2-hydroxy-1-naphthaldimine and its Ni (II) complex,” J. Mol. Struct., vol. 1269, p. 133717, 2022.
18. R. K. Gurung, “Synthesis, Characterization, Spectroscopic, and Mesomorphic Studies of New Schiff Base Ligands and Titanium, Cobalt, Nickel and Copper Metal Centers.” Old Dominion University, 2020.
19. O. A. El-Gammal, D. A. Saad, and A. F. Al-Hossainy, “Synthesis, spectral characterization, optical properties and X-ray structural studies of S centrosymmetric N2S2 or N2S2O2 donor Schiff base ligand and its binuclear transition metal complexes,” J. Mol. Struct., vol. 1244, p. 130974, 2021.

20. M. Nur Amin Bitu, “Anti-pathogenic Activity of Cu(II) Complexes Incorporating Schiff Bases: A Short Review,” Am. J. Heterocycl. Chem., vol. 5, no. 1, p. 11, 2019.
21. T. Rosu et al., “Synthesis, structural and spectral studies of Cu(II) and V(IV) complexes of a novel Schiff base derived from pyridoxal. Antimicrobial activity,” Polyhedron, vol. 31, no. 1, pp. 352–360, Jan. 2012.
22. B. S. Creaven et al., “Anticancer and antifungal activity of copper(II) complexes of quinolin-2(1H)-one-derived Schiff bases,” Inorganica Chim. Acta, vol. 363, no. 14, pp. 4048–4058, Nov. 2010.
23. vahideh Hadigheh-Rezvan and Y. Aminivand, “Dft Computational Study of Optical Properties for Bis-Schiff Bases of 8-Aminoquinoline Derivatives and Furan-2, 3-Di-Carbaldehyde,” SSRN Electron. J., 2022.
24. D. Tamafo Fouegue, J. H. Nono, N. K. Nkungli, and J. N. Ghogomu, “A theoretical study of the structural and electronic properties of some titanocenes using DFT, TD-DFT, and QTAIM,” Struct. Chem., vol. 32, pp. 353–366, 2021.
25. F. Stanzione, I. Giangreco, and J. C. Cole, “Use of molecular docking computational tools in drug discovery,” Prog. Med. Chem., vol. 60, pp. 273–343, 2021.
26. A. Vaseashta, M. Vaclavikova, S. Vaseashta, G. Gallios, P. Roy, and O. Pummakarnchana, “Nanostructures in environmental pollution detection, monitoring, and remediation,” Sci. Technol. Adv. Mater., vol. 8, no. 1–2, p. 47, 2007.
27. M. Hull and D. Bowman, Nanotechnology environmental health and safety: risks, regulation, and management. William Andrew, 2018.
28. F. Ejeian et al., “Biosensors for wastewater monitoring: A review,” Biosens. Bioelectron., vol. 118, pp. 66–79, 2018.
29. R. Khan, V. Patel, and Z. Khan, “Materials in emerging water pollutants detection,” Sensors Water Pollut. Monit. Role Mater., pp. 255–275, 2020.
30. D. E. Babatunde, I. H. Denwigwe, O. M. Babatunde, S. L. Gbadamosi, I. P. Babalola, and O. Agboola, “Environmental and societal impact of nanotechnology,” IEEE Access, vol. 8, pp. 4640–4667, 2019.
31. T. Oymak, Ş. Tokalıoğlu, V. Yılmaz, Ş. Kartal, and D. Aydın, “Determination of lead and cadmium in food samples by the coprecipitation method,” Food Chem., vol. 113, no. 4, pp. 1314–1317, 2009.
32. S. Malik et al., “Nanomaterials-based biosensor and their applications: A review,” Heliyon, vol. 9, no. 9, p. e19929, Sep. 2023.
33. M. Ramesh, R. Janani, C. Deepa, and L. Rajeshkumar, “Nanotechnology-Enabled Biosensors: A Review of Fundamentals, Design Principles, Materials, and Applications,” Biosensors, vol. 13, no. 1, p. 40, Dec. 2022.
34. I. A. Bucurica et al., “Investigation of metallic nanoparticles adsorbed on the QCM sensor by SEM and AFM techniques,” Bull. Mater. Sci., vol. 41, no. 3, p. 71, 2018.
35. L. Manjakkal et al., “Connected sensors, innovative sensor deployment, and intelligent data analysis for online water quality monitoring,” IEEE Internet Things J., vol. 8, no. 18, pp. 13805–13824, 2021.
36. A. Fetoh, K. A. Asla, A. A. El-Sherif, H. El-Didamony, and G. M. A. El-Reash, “Synthesis, structural characterization, thermogravimetric, molecular modeling and biological studies of Co (II) and Ni (II) Schiff bases complexes,” J. Mol. Struct., vol. 1178, pp. 524–537, 2019.
37. E. M. Komyha, W. H. Mahmoud, W. M. Hosny, and A. A. El-Sherif, “Design, Structural Characterization, Molecular docking and Biomedical Applications Of Hydrazone-based Schiff base Metal Complexes,” Egypt. J. Chem., vol. 66, no. 13, pp. 1219–1230, 2023.
38. M. Bayomi, W. H. Mahmoud, M. ElMosallamy, and A. A. El-Sherif, “Schiff base transition metal (II) complexes: spectral analyses and biological application,” Egypt. J. Chem., 2023.
39. H. M. Fahmy, A. M. Mosleh, A. A. El-Sayed, and A. A. El-Sherif, “Novel palladium (II) and Zinc (II) Schiff base complexes: Synthesis, biophysical studies, and anticancer activity investigation,” J. Trace Elem. Med. Biol., p. 127236, 2023.
40. H. M. Fahmy, F. M. Abdel-Rahman, A. A. El-Sayed, and A. A. El-Sherif, “Study of novel bidentate heterocyclic amine-based metal complexes and their biological activities: cytotoxicity and antimicrobial activity evaluation,” BMC Chem., vol. 17, no. 1, p. 78, 2023.
41. M. T. Radwan, W. H. Mahmoud, M. A. F. ElMosallamy, and A. A. El-Sherif, “TRANSITION METAL COMPLEXES INCORPORATING SYMMETRIC tetra dentate Schiff base ligand: Synthesis, characterization, biological activities, DFT and molecular docking studies,” Egypt. J. Chem., vol. 66, no. 13, pp. 1329–1339, 2023.
42. W. Al-Gethami, N. Al-Qasmi, S. H. Ismail, and A. H. Sadek, “QCM-Based MgFe2O4@ CaAlg Nanocomposite as a Fast Response Nanosensor for Real-Time Detection of Methylene Blue Dye,” Nanomaterials, vol. 13, no. 1, p. 97, 2022.
43. A. A. Mohamed, R. El-Sherif, W. H. Mahmoud, and A. A. El-Sherif, “Investigation of Nanostructure of Schiff Base Copper (II) Complex: Synthesis, Characterization, Textural, and Thermal Property Analysis for Evaluating their Effectiveness as Cadmium Sensors with QCM-Based Sensing Method,” Egypt. J. Chem., 2024.
44. M. S. Mansour, W. H. Mahmoud, and A. A. El-Sherif, “Manganese, Cobalt, and Cadmium Complexes of Quinazoline Schiff Base Ligand and Methionine: Synthesis, Characterization, DFT, Docking studies and biomedical application,” Egypt. J. Chem., 2024.
45. M. S. A. Mansour, A. A. El-Sherif, W. H. Mahmoud, and abeer taha, “QCM-Based Nano Schiff base Quinazoline-methionine hybrid ligand complex with Cobalt (II) as a Fast Response Nanosensor for instantaneous Monitoring water pollutant Pb (II) Ions,” Egypt. J. Chem., 2024.
46. P. A. Khalaf-Alla, M. M. Shoukry, M. R. Shehata, A. M. Abdel Wahab, and R. Van Eldik, "Synthesis, equilibrium, DFT, and docking studies of a homopiperazine complex with dibutyltin(IV)," Journal of Coordination Chemistry, vol. 77(7-8), pp. 880-895, 2024.

47. M. T. Radwan, W. H. Mahmoud, M. A. F. ElMosallamy, and A. A. El-Sherif, "TRANSITION METAL COMPLEXES INCORPORATING SYMMETRIC tetra dentate Schiff base ligand: Synthesis, characterization, biological activities, DFT and molecular docking studies," Egypt. J. Chem., vol. 66, no. 13, pp. 1329–1339, 2023.
48. P. Taneja, V. Manjuladevi, and R. K. Gupta, "Detection of cadmium ion in water using films of nanocomposite of functionalized carbon nanotubes and anionic polymer," in AIP Conference Proceedings, AIP Publishing, 2018.
49. A. Shaban and L. Eddaif, "Comparative Study of a sensing platform via functionalized calix [4] resorcinarene Ionophores on QCM resonator as sensing materials for detection of heavy metal ions in aqueous environments," Electroanalysis, vol. 33, no. 2, pp. 336–346, 2021.
50. P. Sun, Y. Chen, M. Yan, and T. Tang, "Enhancement of QCM detection for heavy metal ions based on TGA modified CdTe nanospheres," J. Inorg. Organomet. Polym. Mater., vol. 30, pp. 525–531, 2020.
51. Z.-L. Wei, L. Wang, J.-F. Wang, W.-T. Guo, Y. Zhang, and W.-K. Dong, "Two highly sensitive and efficient salamo-like copper (II) complex probes for recognition of CN−," Spectrochim. Acta Part A Mol. Biomol. Spectrosc., vol. 228, p. 117775, 2020.
52. S. M. Annigeri, M. P. Sathisha, and V. K. Revankar, "Spectroscopic studies of bridged binuclear complexes of Co (II), Ni (II), Cu (II) and Zn (II)," Transit. Met. Chem., vol. 32, no. 1, pp. 81–87, 2007.
53. A. A. El-Sherif and T. M. A. Eldebss, "Synthesis, spectral characterization, solution equilibria, in vitro antibacterial and cytotoxic activities of Cu (II), Ni (II), Mn (II), Co (II) and Zn (II) complexes with Schiff base derived from 5-bromosalicylaldehyde and 2-aminomethylthiophene," Spectrochim. Acta Part A Mol. Biomol. Spectrosc., vol. 79, no. 5, pp. 1803–1814, 2011.
54. S. Y. Abbas, W. M. Basyouni, and K. A. M. El-Bayouki, "Synthesis, characterization and antimicrobial activity of 5-(arylazo) salicylaldimines and their copper (II) complexes," Appl. Organomet. Chem., vol. 32, no. 2, p. e4032, 2018.
55. M. Tümer, D. Ekinci, F. Tümer, and A. Bulut, "Synthesis, characterization and properties of some divalent metal (II) complexes: Their electrochemical, catalytic, thermal and antimicrobial activity studies," Spectrochim. Acta Part A Mol. Biomol. Spectrosc., vol. 67, no. 3–4, pp. 916–929, 2007.
56. K. P. Balasubramanian, K. Parameswari, V. Chinnusamy, R. Prabhakaran, and K. Natarajan, "Synthesis, characterization, electro chemistry, catalytic and biological activities of ruthenium (III) complexes with bidentate N, O/S donor ligands," Spectrochim. Acta Part A Mol. Biomol. Spectrosc., vol. 65, no. 3–4, pp. 678–683, 2006.
57. R. Baošić, A. Radojević, M. Radulović, S. Miletić, M. Natić, and Ž. Tešić, "Relationships between structure, retention and biological activity of some Schiff base ligands and their complexes," Biomed. Chromatogr., vol. 22, no. 4, pp. 379–386, 2008.
58. K. S. Kumar and K. K. Aravindakshan, "Synthesis, cytotoxic, anticancer and antimicrobial activities of some metal complexes of a novel tetradentate Schiff base ligand,(E)-3-((2-((E)-(1-(2-hydroxyphenyl) ethylidene) amino) ethyl) imino)-N-phenylbutanamide," Results Chem., vol. 3, p. 100129, 2021.
59. H. Kargar et al., "Novel copper (II) and zinc (II) complexes of halogenated bidentate N, O-donor Schiff base ligands: Synthesis, characterization, crystal structures, DNA binding, molecular docking, DFT and TD-DFT computational studies," Inorganica Chim. Acta, vol. 514, p. 120004, 2021.
60. K. Nejati, A. Bakhtiari, R. Bikas, and J. Rahimpour, "Molecular and electronic structure, spectroscopic and electrochemical properties of copper (II) complexes: Experimental and DFT studies," J. Mol. Struct., vol. 1192, pp. 217–229, 2019.
61. Y. Zheng, J. J. Neville, and C. E. Brion, "Imaging the electron density in the highest occupied molecular orbital of glycine," Science (80-.)., vol. 270, no. 5237, pp. 786–788, 1995.
62. F. M. Elantabli, M. R. Shehata, A. A. Makhlouf, and L. H. Abdel-Rahman, "Co (II), Ni (II), and Cu (II) complexes derived from 1, 2, 4-triazine: Synthesis, characterization, anticancer activity, DFT, and molecular docking studies with a COVID-19 protein receptor," J. Coord. Chem., vol. 75, no. 5–6, pp. 668–688, 2022.
63. V. A. Pathade, R. H. Waghchaure, B. S. Jagdale, T. B. Pawar, and S. S. Pathade, "Molecular structure, frontier molecular orbital and spectroscopic examination on dihydropyrimidinones: a comparative computational approach," J. Adv. Sci. Res., vol. 11, no. Suppl 2, pp. 64–70, 2020.
64. L. S. Braga, D. H. S. Leal, K. Kuca, and T. C. Ramalho, "Perspectives on the role of the frontier effective-for-reaction molecular orbital (FERMO) in the study of chemical reactivity: an updated review," Curr. Org. Chem., vol. 24, no. 3, pp. 314–331, 2020.
65. M. Khajehzadeh and N. Sadeghi, "Molecular structure, the effect of solvent on UV–vis and NMR, FT–IR and FT–Raman spectra, NBO, frontier molecular orbital analysis of Mitomycin anticancer drug," J. Mol. Liq., vol. 256, pp. 238–246, 2018.
66. F. Akman, "A density functional theory study based on monolignols: Molecular structure, HOMO-LUMO analysis, molecular electrostatic potential," Transport, vol. 1, p. 2, 2019.
67. S. Lakshminarayanan, V. Jeyasingh, K. Murugesan, N. Selvapalam, and G. Dass, "Molecular electrostatic potential (MEP) surface analysis of chemo sensors: An extra supporting hand for strength, selectivity & non-traditional interactions," J. Photochem. Photobiol., vol. 6, p. 100022, 2021.
68. D. A. Nassar, M. R. Shehata, and A. S. S. Sayed, "Structural Characterization, DFT Calculations, Metal Uptake, Fluorescence, Antimicrobial and Molecular Docking Studies of Novel Co (II) and Ni (II) Complexes with NNS Tridentate Schiff base Ligand," 2022.
69. Z. un Nisa, A. Gul, Z. Akhter, M. A. Nadeem, M. N. Tahir, and M. U. Ahmed, "Some newly synthesized ferrocene based esters: Characterization, DNA interaction and DFT studies," J. Organomet. Chem., vol. 820, pp. 130–140, 2016.

70. A. A. El-Sherif, A. Fetoh, Y. K. Abdulhamed, and G. M. A. El-Reash, "Synthesis, structural characterization, DFT studies and biological activity of Cu (II) and Ni (II) complexes of novel hydrazone," Inorganica Chim. Acta, vol. 480, pp. 1–15, 2018.
71. A. M. Shehabeldine et al., "Potential antimicrobial and antibiofilm properties of copper oxide nanoparticles: time-kill kinetic essay and ultrastructure of pathogenic bacterial cells," Appl. Biochem. Biotechnol., vol. 195, no. 1, pp. 467–485, 2023.
72. O. Maťátková, J. Michailidu, A. Miškovská, I. Kolouchová, J. Masák, and A. Čejková, "Antimicrobial properties and applications of metal nanoparticles biosynthesized by green methods," Biotechnol. Adv., vol. 58, p. 107905, 2022.
73. S. Hemmati, A. Ahmeda, Y. Salehabadi, A. Zangeneh, and M. M. Zangeneh, "Synthesis, characterization, and evaluation of cytotoxicity, antioxidant, antifungal, antibacterial, and cutaneous wound healing effects of copper nanoparticles using the aqueous extract of Strawberry fruit and L-Ascorbic acid," Polyhedron, vol. 180, p. 114425, 2020.
74. A. A. Mohamed, M. Abu-Elghait, N. E. Ahmed, and S. S. Salem, "Eco-friendly mycogenic synthesis of ZnO and CuO nanoparticles for in vitro antibacterial, antibiofilm, and antifungal applications," Biol. Trace Elem. Res., vol. 199, pp. 2788–2799, 2021.
75. E. M. Zayed, G. G. Mohamed, and A. M. M. Hindy, "Transition metal complexes of novel Schiff base: Synthesis, spectroscopic characterization, and in vitro antimicrobial activity of complexes," J. Therm. Anal. Calorim., vol. 120, pp. 893–903, 2015.
76. M. S. Aljahdali and A. A. El-Sherif, "Synthesis and biological evaluation of novel Zn (II) and Cd (II) Schiff base complexes as antimicrobial, antifungal, and antioxidant agents," Bioinorg. Chem. Appl., vol. 2020, pp. 1–17, 2020.
77. A. A. Hamed, A. A. El-Sherif, C. M. Sharaby, Y. A. Ammar, and M. F. Amine, "SYNTHESIS OF NEW LIGAND-BASED PHOSPHAZO RING AND ITS TRANSITION METAL COMPLEXES AS CANCER INHIBITOR: SPECTROSCOPIC, DFT, ANTIMICROBIAL, AND MOLECULAR DOCKING INVESTIGATIONS," Al-Azhar Bull. Sci., vol. 34, no. 2, p. 4, 2023.
78. L. H. Abdel-Rahman, A. M. Abu-Dief, R. M. El-Khatib, and S. M. Abdel-Fatah, "Some new nano-sized Fe (II), Cd (II) and Zn (II) Schiff base complexes as precursor for metal oxides: Sonochemical synthesis, characterization, DNA interaction, in vitro antimicrobial and anticancer activities," Bioorg. Chem., vol. 69, pp. 140–152, 2016.
79. M. Mansour, F. E.-T. Heakal, and A. El-sherif, "Potentiometric, Thermodynamics, and Modeling Investigates of Binary and Ternary Zn (Ii) Complexes Prepared from 1-H-Benzimidazole-2-Carboxylic Acid and Some Biologically Active Ligands," Fakiha El-Taib El-sherif, Ahmed, Potentiometric, Thermodyn. Model. Investig. Bin. Ternary Zn Complexes Prep. From, 2024.
80. D. Domyati, S. A. Zabin, A. A. Elhenawy, and M. Abdelbaset, "Preparation, Antimicrobial Activity and Docking Study of Vanadium Mixed Ligand Complexes Containing 4-Amino-5-hydrazinyl-4 H-1, 2, 4-triazole-3-thiol and Aminophenol Derivatives," Processes, vol. 9, no. 6, p. 1008, 2021.
81. M. A. El-Ghamry, F. M. Elzawawi, A. A. A. Aziz, K. M. Nassir, and S. M. Abu-El-Wafa, "New Schiff base ligand and its novel Cr (III), Mn (II), Co (II), Ni (II), Cu (II), Zn (II) complexes: Spectral investigation, biological applications, and semiconducting properties," Sci. Rep., vol. 12, no. 1, p. 17942, 2022.
82. Q. Xiao et al., "High-resolution X-ray structure of three microtubule-stabilizing agents in complex with tubulin provide a rationale for drug design," Biochem. Biophys. Res. Commun., vol. 534, pp. 330–336, 2021.
83. H. E. Swanson, Standard X-ray diffraction powder patterns, vol. 25. US Department of Commerce, National Bureau of Standards, 1953.
84. S. Mourdikoudis, R. M. Pallares, and N. T. K. Thanh, "Characterization techniques for nanoparticles: comparison and complementarity upon studying nanoparticle properties," Nanoscale, vol. 10, no. 27, pp. 12871–12934, 2018.
85. B. S. Murty and S. Ranganathan, "Novel materials synthesis by mechanical alloying/milling," Int. Mater. Rev., vol. 43, no. 3, pp. 101–141, 1998.
86. L. Angeloni, D. Passeri, P. G. Schiavi, F. Pagnanelli, and M. Rossi, "Magnetic force microscopy characterization of cobalt nanoparticles: A preliminary study," in AIP Conference Proceedings, AIP Publishing, 2020.
87. S. Bhattacharjee, "DLS and zeta potential–what they are and what they are not?," J. Control. release, vol. 235, pp. 337–351, 2016.
88. J. Jiang, G. Oberdörster, and P. Biswas, "Characterization of size, surface charge, and agglomeration state of nanoparticle dispersions for toxicological studies," J. Nanoparticle Res., vol. 11, pp. 77–89, 2009.
89. P. Zhang, L. Wang, J. Xie, L. Su, and C. Ma, "Micro/nano-complex-structure SiO x–PANI–Ag composites with homogeneously-embedded Si nanocrystals and nanopores as high-performance anodes for lithium-ion batteries," J. Mater. Chem. A, vol. 2, no. 11, pp. 3776–3782, 2014.
90. H. Rajabi, S. M. Jafari, J. Feizy, M. Ghorbani, and S. A. Mohajeri, "Preparation and characterization of 3D graphene oxide nanostructures embedded with nanocomplexes of chitosan-gum Arabic biopolymers," Int. J. Biol. Macromol., vol. 162, pp. 163–174, 2020.
91. M. Szafraniec and D. Barnat-Hunek, "Evaluation of the contact angle and wettability of hydrophobised lightweight concrete with sawdust," Bud. i Archit., vol. 19, no. 2, 2020.
92. S. S. Gavande, Y. H. Navale, A. S. Salunkhe, S. Gavande, P. S. Kulkarni, and B. R. Karche, "Investigation of Supercapacitive Behaviour of Electrodeposited Cobalt Oxide Thin Film by Potentiostatic Mode," J. Nano-and Electron. Phys., vol. 12, no. 2, 2020.
93. M. M. Sayed, Z. I. Nabil, N. S. El-Shenawy, R. A. Al-Eisa, and M. S. Nafie, "In Vitro and In Vivo Effects of Synthesis Novel Phenoxyacetamide Derivatives as Potent Apoptotic Inducer against HepG2 Cells through PARP-1 Inhibition," Pharmaceuticals, vol. 16, no. 11, p. 1524, 2023.

94. E. T. Nagy et al., “Design and cytotoxic evaluation via apoptotic and antiproliferative activity for novel 11 (4-aminophenylamino) neocryptolepine on hepatocellular and colorectal cancer cells,” Apoptosis, vol. 28, no. 3–4, pp. 653–668, 2023.
95. Q. Yao, J. Xie, J. Liu, H. Kang, and Y. Liu, “Adsorption of lead ions using a modified lignin hydrogel,” J. Polym. Res., vol. 21, pp. 1–16, 2014.
96. N. A. A. Qasem, R. H. Mohammed, and D. U. Lawal, “Removal of heavy metal ions from wastewater: A comprehensive and critical review,” Npj Clean Water, vol. 4, no. 1, p. 36, 2021.
97. S. M. M. Hizam, A. M. Al-Dhahebi, and M. S. Mohamed Saheed, “Recent advances in graphene-based nanocomposites for ammonia detection,” Polymers (Basel)., vol. 14, no. 23, p. 5125, 2022.
98. S. N. A. Mustaffa et al., “Sensing mechanism of an optimized room temperature optical hydrogen gas sensor made of zinc oxide thin films,” J. Mater. Res. Technol., vol. 9, no. 5, pp. 10624–10634, 2020.
99. D. R. Boverhof and R. M. David, “Nanomaterial characterization: considerations and needs for hazard assessment and safety evaluation,” Anal. Bioanal. Chem., vol. 396, pp. 953–961, 2010.
100. M. R. Hassan and M. I. Aly, “Magnetically synthesized MnFe2O4 nanoparticles as an effective adsorbent for lead ions removal from an aqueous solution,” AQUA—Water Infrastructure, Ecosyst. Soc., vol. 70, no. 6, pp. 901–920, 2021.
101. L. Chaabane, E. Beyou, A. El Ghali, and M. H. V Baouab, “Comparative studies on the adsorption of metal ions from aqueous solutions using various functionalized graphene oxide sheets as supported adsorbents,” J. Hazard. Mater., vol. 389, p. 121839, 2020.
102. Z. Raji, A. Karim, A. Karam, and S. Khalloufi, “Adsorption of heavy metals: Mechanisms, kinetics, and applications of various adsorbents in wastewater remediation—A review,” in Waste, MDPI, 2023, pp. 775–805.
103. F. Ergüvenerler, Ş. Targan, and V. N. Tirtom, “Removal of lead from aqueous solutions by low cost and waste biosorbents (lemon, bean and artichoke shells),” Water Sci. Technol., vol. 81, no. 1, pp. 159–169, 2020.
104. L. H. Abdel-Rahman, M. R. Shehata, E. A. H. Ahmed, K. M. Mohammed, and A. Nafady, "Facile synthesis and grafting of N2O2-Cu (II) Schiff base complex onto graphene oxide surface: Aspects of its antimicrobial, anticancer, antiCOVID-19 and photodegradation of methylene blue," Vietnam Journal of Chemistry, Vol. 62(2), pp.178-194, 2024.
105. E. M. W. H. M. W. M. H. and A. A. E.-S. Komyha, “Design and Characterization of Nano Cobalt Complex As Low Limit Detection Qcm Sensor for Cadmium Ions,” Egypt. J. Chem, vol. 67, no. 5, pp. 1–2, 2024.